CRISPR Screens Identify Novel Regulators of cFLIP Dependency and Ligand-Independent, TRAIL-R1-Mediated Cell Death

Neil Kuehnle[1], Scout Mask Osborne[1], Ziyan Liang[1], Mark Manzano[2], and Eva Gottwein[1]

*Corresponding author, email: e-gottwein@northwestern.edu; phone: 312-503-3075

[1]Department of Microbiology-Immunology, Northwestern University, Feinberg School of Medicine, Tarry 6-735, Chicago, Illinois, 60611, USA

[2]Current Address: Mark Manzano, Department of Microbiology and Immunology, University of Arkansas for Medical Sciences, Little Rock, Arkansas, USA.

Abstract

Kaposi's sarcoma-associated herpesvirus (KSHV) causes primary effusion lymphoma (PEL). PEL cell lines require expression of the cellular FLICE inhibitory protein (cFLIP) for survival, although KSHV encodes a viral homolog of this protein (vFLIP). Cellular and viral FLIP proteins have several functions, including, most importantly, the inhibition of pro-apoptotic caspase 8 and modulation of NF-κB signaling. To investigate the essential role of cFLIP and its potential redundancy with vFLIP in PEL cells, we first performed rescue experiments with human or viral FLIP proteins known to affect FLIP target pathways differently. The long and short isoforms of cFLIP and molluscum contagiosum virus MC159L, which are all strong caspase 8 inhibitors, efficiently rescued the loss of endogenous cFLIP activity in PEL cells. KSHV vFLIP was unable to fully rescue the loss of endogenous cFLIP and is therefore functionally distinct. Next, we

employed genome-wide CRISPR/Cas9 synthetic rescue screens to identify loss of function perturbations that can compensate for cFLIP knockout. Results from these screens and our validation experiments implicate the canonical cFLIP target caspase 8 and TRAIL receptor 1 (TRAIL-R1 or TNFRSF10A) in promoting constitutive death signaling in PEL cells. However, this process was independent of TRAIL receptor 2 or TRAIL, the latter of which is not detectable in PEL cell cultures. The requirement for cFLIP is also overcome by inactivation of the ER/Golgi resident chondroitin sulfate proteoglycan synthesis and UFMylation pathways, Jagunal homolog 1 (JAGN1) or CXCR4. UFMylation and JAGN1, but not chondroitin sulfate proteoglycan synthesis or CXCR4, contribute to TRAIL-R1 expression. In sum, our work shows that cFLIP is required in PEL cells to inhibit ligand-independent TRAIL-R1 cell death signaling downstream of a complex set of ER/Golgi-associated processes that have not previously been implicated in cFLIP or TRAIL-R1 function.

Introduction

Primary effusion lymphoma (PEL) is a non-Hodgkin lymphoma comprised of KSHV-transformed B cells that typically accumulate in body cavities[1, 2]. PEL is primarily seen in HIV/AIDS patients and has a poor prognosis, with an average survival below two years[3]. Although the etiology of PEL is incompletely understood, latently expressed KSHV oncoproteins are thought to play essential roles in the KSHV-mediated transformation of PEL cells, including the latency-associated nuclear antigen (LANA), viral interferon regulatory factor 3 (vIRF3), a KSHV-encoded D type cyclin (vCyc), and viral FLICE-inhibitory protein (vFLIP). Indeed, cultured patient derived PEL cell lines depend on the continued expression of several latency genes[4, 5]. vFLIP is considered a major candidate for a viral driver of KSHV-mediated B cell transformation in PEL due to its well-documented ability to activate NF-κB survival signaling[6]. A previous study by our lab explored the dependency of PEL cell lines on cellular genes using genome-wide

49 CRISPR knockout screens[7]. This study identified a surprising dependency on cellular FLIP
50 (cFLIP, encoded by *CFLAR*), despite the presence of the KSHV-encoded vFLIP locus. This
51 study furthermore showed that only two of eight tested PEL cell lines depended on genes
52 related to NF-κB signaling. These unexpected findings prompted us to further investigate the
53 role of cFLIP in the context of KSHV-transformed PEL cell lines and to differentiate it from that
54 of vFLIP.
55 Canonically, FLIP proteins act as dominant-negative inhibitors of caspase 8 (*CASP8*)-induced
56 apoptosis by preventing formation of the death-inducing signaling complex (DISC) or directly
57 inhibiting active CASP8[8, 9, 10, 11]. Non-canonical cFLIP activities have been identified, including
58 the regulation of NF-κB signaling[6, 12]. While KSHV vFLIP is a strong activator of NF-κB signaling,
59 it is currently unclear whether vFLIP is a potent inhibitor of CASP8[13, 14, 15]. CASP8 is a pro-
60 apoptotic protein in the cysteine protease (caspase) family that typically acts as the initiator
61 caspase in the extrinsic apoptotic pathway induced by the death ligands tumor necrosis factor α
62 (TNFα), Fas ligand, or TNF-related apoptosis-inducing ligand (TRAIL) (as reviewed in [16]). The
63 binding of these ligands to their specific death receptors initiates the formation of the death-
64 inducing signaling complex (DISC), containing Fas-associated death domain (FADD) protein
65 and inactive pro-CASP8. Autocatalytic cleavage of pro-CASP8 in DISC generates active
66 CASP8, which initiates apoptosis. However, additional cellular processes converge on CASP8
67 to regulate cell death, including necroptosis, pyroptosis, autophagy-dependent cell death, and
68 hyperactivation of the ER stress pathway/the unfolded protein response (UPR) [17, 18, 19, 20, 21, 22].

69 Here, we sought to clarify the respective roles of cFLIP and vFLIP in PEL. Our results show that
70 vFLIP is robustly expressed only in a subset of PEL cell lines, which also depend on genes that
71 function in NF-κB signaling. The tight correlation of vFLIP expression with NF-κB dependency in
72 PEL cell lines suggests that vFLIP functions in its well-established role as an activator of the
73 NF-κB pathway in PEL. vFLIP cannot fully compensate for the absence of cFLIP, pointing to a

74 non-redundant function of cFLIP in PEL cells. Using genetic screening and validation
75 experiments, we established that cFLIP is required to inhibit ligand-independent, constitutive
76 death signaling by one of the TRAIL receptors, TRAIL-R1 (encoded by *TNFRSF10A*).

77

78 **Results**

79 **vFLIP expression is variable in PEL cell lines**

80 We first examined the expression of human cFLIP and cyclin D2 and their viral homologs vFLIP
81 and vCyc across 8 PEL cell lines and the KSHV-negative B cell line BJAB. As a control, we
82 analyzed KSHV vIRF3, which is latently expressed in PEL from a distinct KSHV locus[4]. We
83 observed comparable expression of the major isoforms of cFLIP, cyclin D2, and KSHV vIRF3
84 across the PEL cell lines (Fig. 1A). In contrast, vFLIP and vCyc expression varied greatly, with
85 vFLIP expression detected only in BC-1 and BC-3. Importantly, these are the same two PEL cell
86 lines shown to depend on NF-κB signaling genes in our previous study of cellular gene
87 dependency in PEL cells (Fig. 1A, bottom)[7]. vCyc expression mirrored the expression of vFLIP,
88 as expected due to their bicistronic expression[23], with the surprising exception of BC-2. Serial
89 dilution of BC-3 lysates suggested that our Western protocol is sensitive enough to detect vFLIP
90 and vCyc expression levels that are ~20-50 fold below those of BC-3 (Fig. S1A, B). The
91 observed patterns of vFLIP expression and NF-κB dependency are consistent with the
92 published role of vFLIP in the activation of NF-κB survival signaling[6, 15, 24, 25, 26, 27], in the subset
93 of PEL cell lines where vFLIP is expressed.

94 **cFLIP is broadly essential in PEL cell lines**

95 We previously validated cFLIP dependency of the PEL cell line BCBL-1[7]. To establish cFLIP
96 dependency more broadly across PEL cell lines, we performed single guide RNA (sgRNA)-
97 induced functional inactivation (KO) of cFLIP followed by cumulative growth curve analysis

98 relative to an sgRNA that targets a safe harbor locus (sgAAVS1) in BCBL-1/Cas9 and 4
99 additional Cas9-expressing PEL cell lines (Fig. 1B, Fig. S1C). sgRNAs against the proteasomal
100 subunit PSMD1 and the transcription factor IRF4 served as positive controls for well-established
101 essential genes in PEL cells. The cFLIP sgRNAs lack homology to vFLIP and did not affect
102 vFLIP expression in BC-3 cells (Fig. S1D). For BC-1, which did not show significant depletion of
103 cFLIP-specific sgRNAs in our original CRISPR knockout screens (Fig. 1A, [7]), the experiment
104 was done in a Cas9 cell clone with improved gene editing compared to the original cell pool[7].
105 Results showed that in addition to BCBL-1, BC-1, BC-2, and BC-5 require cFLIP for viability.
106 Thus, BC-1 was false negative for cFLIP dependency in our original CRISPR screens[7]. In
107 contrast, cFLIP single gene KO did not significantly affect the viability of BC-3 cells. Cell death
108 following cFLIP KO in BCBL-1/Cas9 cells was rescued by lentiviral re-expression of either major
109 cFLIP isoform (cFLIP-L and S; Figs. 1C, S1E). These data collectively confirm that cFLIP is
110 essential in the majority of PEL cell lines. The essentiality of cFLIP in BC-1 furthermore
111 suggests that expression of vFLIP may not be sufficient to overcome the requirement for cFLIP.

112 **cFLIP and vFLIP have distinct roles in PEL cell lines**

113 To further investigate whether vFLIP and cFLIP are redundant, we tested if KSHV vFLIP can
114 rescue cells from cell death after cFLIP KO. We additionally tested the viral FLIP proteins
115 encoded by molluscum contagiosum virus (MCV), MC159L or MC160L, given that KSHV vFLIP
116 and MCV MC159L and MC160L each have distinct functional activities (Fig. 2A). While either
117 major isoform of cFLIP can inhibit CASP8 and activate NF-κB signaling in ectopic contexts[12, 28,
118 29, 30], reports of KSHV vFLIP's ability to strongly inhibit CASP8 are mixed or ambiguous.
119 Conversely, MCV MC159L and MC160L both repress NF-κB signaling and only MC159L inhibits
120 CASP8[8, 31, 32, 33]. Thus, this approach allows us to assess the redundancy of vFLIP with cFLIP
121 and the importance of NF-κB activation and CASP8 inhibition for cFLIP dependency.

122 Interestingly, we observed only partial rescue of cFLIP dependency after overexpression of
123 KSHV vFLIP (Figs. 2B, C, S2A). In contrast, overexpression of MC159L conferred complete
124 rescue, while overexpression of MC160L had no effect. Expression of each of the viral FLIP
125 proteins was comparable to overexpressed cFLIP and did not affect the expression of
126 endogenous cFLIP (Figs. S2A, B). KSHV vFLIP was furthermore overexpressed well above
127 levels of the endogenous viral protein in BC-3 (Fig. S2C). Thus, the inability of vFLIP to
128 efficiently rescue cFLIP expression is not due to lower expression relative to cFLIP or
129 endogenous vFLIP. Collectively, these results suggest that FLIP proteins that are known potent
130 inhibitors of CASP8 (cFLIP and MC159L), but not KSHV vFLIP, can efficiently rescue cFLIP
131 dependency in PEL cells. Therefore, the essential role of cFLIP in PEL cells is substantially
132 distinct from that of vFLIP.

133 **Genome-wide rescue screens uncover an ER/Golgi/CASP8-dependent death signaling**
134 **program repressed by cFLIP**

135 cFLIP has a well-characterized role in protecting cells from the effects of cell death ligands of
136 the extrinsic apoptosis pathway[9, 11]. Indeed, Epstein-Barr virus (EBV)-immortalized
137 lymphoblastoid cell lines (LCLs) depend on cFLIP expression for protection from autocrine TNF-
138 α signaling[34]. TNF-α is not expressed in PEL cell lines (Fig. S3), however. We therefore sought
139 to identify mechanisms underlying cFLIP dependency of PEL cell lines in genome-wide
140 CRISPR/Cas9 rescue screens, outlined in Fig. 3A. In these screens, sgRNAs targeting genes
141 whose inactivation overcomes cFLIP dependency should be enriched after toxic cFLIP
142 inactivation and may represent putative components of the cell death process that is inhibited by
143 cFLIP in PEL cells. We initially chose the background of BCBL-1/Cas9, which has strong cFLIP
144 dependency and excellent CRISPR/Cas9 editing efficiency. Briefly, we transduced BCBL-
145 1/Cas9 with the genome-wide Brunello sgRNA library[35] and passaged the cell population to
146 allow dropout of sgRNAs targeting essential genes. We next challenged the resulting cell pool

147 with another sgRNA vector targeting either cFLIP or the AAVS1 safe harbor locus and further
148 passaged the culture until a cFLIP-sgRNA resistant population was obtained (Fig. S4A). In an
149 independent experiment, we used three separate shRNAs for toxic cFLIP knock-down alongside
150 two negative control shRNAs targeting Renilla luciferase (RLuc) (Fig. S4B). We finally repeated
151 the sg-cFLIP resistance screen in BC-2, which has robust cFLIP dependency (Fig. 1A, B). In
152 each case, resulting cell pools were subjected to next generation sequencing of the Brunello
153 sgRNA inserts and sgRNA composition was analyzed using MAGeCK's robust ranked
154 aggregation (RRA) (Table S1). Independent shRNAs targeting either cFLIP or RLuc were
155 treated as replicates in this analysis. Results from the BCBL-1/Cas9 screens were more robust
156 than those from the BC-2 screen, which was noisy, most likely due to relatively poor editing in
157 the BC-2 Cas9 cell pool (Fig. S4C). Within BCBL-1, top hits from the shRNA-based challenge
158 were statistically more significant but had less dramatic sgRNA fold-changes (Fig. S4C). This is
159 likely due to the inclusion of three different shRNAs targeting cFLIP, each resulting in less
160 complete toxicity than the single highly efficient cFLIP sgRNA (Fig. S4A, B). To account for
161 these differences, we initially compared the BCBL-1 sgRNA and shRNA screens using a rank-
162 based filtering approach. Intersecting the top 150 hits by RRA score from the sgRNA and
163 shRNA challenge in BCBL-1 yielded 23 high-confidence hits (Fig. 3B, Table S2).

164 DAVID pathway analysis[36] shows that these high confidence hits function in three main
165 pathways (Table S3, Fig. 3C): the extrinsic apoptosis pathway (including CASP8, FADD, and
166 TNFRSF10A, encoding TRAIL receptor 1, Fig. 3D), protein modification by the ubiquitin-like
167 modifier UFM1 (UFMylation, Fig. 3E), and chondroitin sulfate proteoglycan synthesis (Fig. 3F).
168 Hits were furthermore enriched for genes associated with the ER and Golgi cellular
169 compartments (Fig. 3C). Specifically, TRAIL-R1 and CXCR4 are transmembrane receptors
170 which traffic through the ER-Golgi network. The UFMylation pathway mediates ubiquitin-fold
171 modified 1 (UFM1) conjugation to lysine residues of target proteins at the cytoplasmic surface of

172 the ER membrane[37, 38, 39, 40, 41, 42, 43]. SRP68 and SRP72 are components of the signal
173 recognition peptide (SRP) complex, which cooperates with the SEC61A translocon to aid
174 insertion of nascent transmembrane proteins into the ER[44, 45, 46] (Fig. 3E). The SRP is involved
175 in translational halting during membrane insertion[46, 47]. ER translocation of translationally
176 paused nascent peptides requires UFMylation of the 60S ribosomal protein L26 (RPL26), which
177 has been proposed as the primary target of UFM1 modification[48, 49]. Nine of the 23 high
178 confidence hits participate in the chondroitin sulfate proteoglycan synthesis pathway (Fig. 3F), a
179 process that occurs in the Golgi apparatus and involves the addition of chondroitin sulfate
180 moieties to transmembrane proteins[50]. Jagunal homolog 1 (JAGN1) is required for vesicular
181 transport from the ER or Golgi, although the exact step JAGN1 participates in is unclear[51].
182 Lastly, EHMT2 is a histone methyltransferase which has been implicated in the epigenetic
183 regulation of the UPR and/or ER homeostasis[52, 53]. A subset of these genes also scored in the
184 top 150 hits of the BC-2 screen, including CASP8 and TNFRSF10A (extrinsic apoptosis), UBA5
185 and UFSP2 (UFMylation), and UXS1, B4GALT7, CHST15, CSGALNACT1 (chondroitin sulfate
186 proteoglycan synthesis), thereby confirming these genetic interactions of cFLIP in a second PEL
187 cell line (Tables S1 and S2).

188 Consistent with our screening results, BCBL-1 CASP8 KO pools derived using two different
189 sgRNAs were completely protected from cell death after subsequent cFLIP sgRNA challenge
190 (Figs. 4, Fig. S4D). These results confirm that our screens capture CASP8 as a key component
191 of the cell death pathway that necessitates cFLIP expression in PEL cells.

192 **cFLIP protects PEL cells from ligand-independent TRAIL-R1-induced cell death**

193 In addition to *CASP8*, *TNFRSF10A,* encoding TRAIL receptor 1 (TRAIL-R1/DR4) scored highly
194 in our screens. Interestingly, neither the ligand for TRAIL-R1 (i.e. *TNFSF10* encoding TRAIL)
195 nor *TNFRSF10B*, encoding TRAIL receptor 2 (TRAIL-R2/DR5), or other death receptors were
196 hits in our screens (Table S1). As for CASP8, we generated TRAIL-R1 KO pools using two

197 independent sgRNAs (Fig. 5A). Cumulative growth curve analyses following subsequent cFLIP
198 KO confirmed that TRAIL-R1-deficient cells no longer require cFLIP expression for viability (Fig.
199 5B, Fig. S5A). TRAIL (ligand) mRNA is not well expressed in RNA-seq data from three different
200 PEL cell lines, including BCBL-1 (Fig S3). Indeed, TRAIL ELISA on cellular supernatants or
201 lysates of BCBL-1 and BC-3 cells failed to detect secreted or intracellular TRAIL[54, 55] in either
202 cell line (Fig. 5C). This assay detected levels of recombinant TRAIL well below the IC50 of
203 "TRAIL-sensitive" cell lines within the literature[56]. BCBL-1 cells are furthermore TRAIL-resistant,
204 even to hyper-physiological concentrations as high as 10 µg/mL (Fig. S5B). As additional
205 controls, we generated TRAIL and TRAIL-R2 KO pools. While NGS-based sequencing of the
206 targeted loci to characterize indel rates within our KO pools showed that >95% of each locus
207 contains inactivating indels after editing (Table S4), genetic disruption of neither locus affected
208 BCBL-1 dependency on cFLIP (Figs. 5B, S5A).

209 Ligand-independent activation of TRAIL-R2, and in some cases TRAIL-R1, has previously been
210 described within the context of Golgi and ER stress-induced cell death[22, 57, 58, 59, 60, 61]. Ligand
211 independent signaling of TRAIL receptor was proposed to follow the intracellular accumulation
212 of TRAIL-R1 in the Golgi or TRAIL-R2 in the ER-Golgi intermediary compartment (ERGIC)[61, 62].
213 Similarly, TRAIL-R1 in BCBL-1 is exclusively expressed intracellularly in PEL cells (Figs. 5D,
214 S5C). TRAIL-R1 in BCBL-1/Cas9-sgAAVS1 colocalized with the ER marker ERp72 and the cis-
215 Golgi marker Giantin, but much less extensively with the ERGIC marker ERGIC53 (Fig. 5E-F,
216 S5E). A recent study in HCT116 cells has shown that a misfolded mutant of myelin protein zero
217 (MPZ-DelS63) binds to TRAIL-R2 in the ERGIC and consequently triggers TRAIL-independent
218 cell death, while MPZ-DelS63-EctoYtoE misfolds but does not interact with TRAIL-R2[62]. TRAIL-
219 R1 did not colocalize with either form of MPZ in BCBL-1 after their doxycycline (DOX)-inducible
220 expression with a C-terminal mCherry tag (Fig. 5F, S5D). Neither protein furthermore impaired
221 the viability of BCBL-1 cells over the course of several days (not shown). Based on these

222 findings, we conclude that cFLIP protects PEL cells from an intracellular, ligand-independent,
223 TRAIL-R1-mediated cell death program originating within the Golgi or ER.

224 **UFMylation and JAGN1 promote TRAIL-R1 expression in PEL cells**

225 To extend validation of the resistance screens beyond TRAIL-R1 and CASP8, we chose two
226 hits from the UFMylation pathway (UFM1, DDRGK1), two genes from the chondroitin sulfate
227 proteoglycan synthesis pathway (UGDH, CHST15), JAGN1, and CXCR4 for single gene KO by
228 two independent sgRNAs each. Generation of an SRP68 KO cell line failed due to the
229 essentiality of this gene in PEL cells, which was unsurprising since all six subunits of the full
230 SRP complex are pan-essential based on data from the Cancer Dependency Map (Table S2).
231 Regardless, we speculate that the screens correctly captured a biologically relevant connection
232 to the SRP, due to the functional link between the SRP and UFMylation of RPL26. The
233 essentiality of the SRP complex likely also explains why only 2 of 6 SPR complex members
234 scored in our screen (Fig. 3B). We did not attempt generating an EHMT2 KO cell pool, since
235 EHMT2 is also pan-essential and likely essential in PEL cells[7]. Western Blot analysis confirmed
236 disruption of UFMylation in UFM1 KO pools (Fig. S6A). Interestingly, DDRGK1 KO did not
237 reduce the most prominent UFM1-modified bands, suggesting that these represent upstream
238 UFMylation pathway intermediates and/or other DDRGK1-independent UFMylation events. We
239 furthermore confirmed robust editing in all cell pools by indel sequencing (Table S4). We
240 obtained significant rescue from lethal cFLIP KO challenge for every hit, as predicted by our
241 screens (Figs. 6A, Fig. S6B).

242 UFMylation (UFM1 and DDRGK1) and JAGN1 were furthermore required for expression of
243 TRAIL-R1, a type I transmembrane protein that contains an ER signal peptide (Fig. 6B). In
244 contrast, KO of CXCR4 and chondroitin sulfate proteoglycan synthesis pathway genes (UGDH,
245 CHST15) did not affect total TRAIL-R1 or CASP8 expression (Fig. 6B). Furthermore, none of
246 the KOs we tested led to a redistribution of TRAIL-R1 to the cell surface from its typical

247 intracellular location in PEL cells, in contrast to the recently reported redistribution of TNFRSF17
248 after SEC61A inhibition by others (Fig. S6C)[63]. TRAIL-R1 mRNA levels in the knockout cell
249 lines with reduced TRAIL-R1 protein levels were unchanged, indicating that reduced TRAIL-R1
250 expression is not due to changes in transcription or mRNA abundance (Fig. S6D).

251 While CXCR4 is best known for its role as a chemokine receptor and well expressed in PEL
252 RNA-seq data, expression of its ligand, CXCL12, is not detectable in BC-1, BC-3, or BCBL-1
253 cells (Fig. S7A). To establish whether CXCR4 signaling is involved in the rescue phenotype, we
254 tested if CXCR4 inhibitor (AMD3100) treatment overcomes the dependency on cFLIP, using
255 BCBL-1 cells with Dox-inducible Cas9 expression[64]. In these experiments, CXCR4 inhibitor
256 treatment failed to recapitulate the genetic CXCR4 KO effect (Fig S7B-C). This result and the
257 lack of endogenous CXCL12 expression suggest that the role of CXCR4 in triggering TRAIL-R1-
258 dependent cell death in PEL is unrelated to its normal signaling activity.

259 In sum, our data suggest that UFMylation and JAGN1 are required for TRAIL-R1 expression,
260 while CXCR4 and the chondroitin sulfate proteoglycan synthesis pathway may promote TRAIL-
261 R1 signaling or affect cFLIP essentiality by other mechanisms.

262 **Discussion**

263 Here we have distinguished the roles of KSHV vFLIP and human cFLIP in KSHV-transformed
264 PEL cell lines. While cFLIP is required for its canonical function to inhibit CASP8 downstream of
265 a death receptor signal, vFLIP was surprisingly not detected in all PEL cell lines and could not
266 fully compensate for loss of cFLIP expression. Moreover, detectable vFLIP expression
267 correlated with requirements for NF-κB-related genes, consistent with the well characterized
268 role of KSHV vFLIP as an activator of NF-κB signaling. Thus, our data demonstrate that vFLIP
269 and cFLIP have only limited functional overlap in a physiological context. Our results suggest
270 that vFLIP has either low affinity to CASP8 or cannot effectively inhibit CASP8 once bound.

271 Since we achieved very high levels of vFLIP overexpression in our rescue experiments, vFLIP
272 sequestration from CASP8 by NEMO is less likely, although possible. These possibilities should
273 be tested in future studies.

274 We identified TRAIL-R1, but not TRAIL-R2, as the critical death receptor that triggers CASP8-
275 induced cell death in the absence of cFLIP. Unlike in EBV-transformed LCLs[34], this process
276 appears entirely ligand independent. Interestingly, such a ligand-independent process has been
277 described in response to ER stress-induced cell death, mainly for TRAIL-R2. A ligand-
278 independent role for TRAIL-R1 has also been reported, but primarily in the context of added
279 Golgi and/or secretory stressors rather than general ER stress[22, 57, 58, 59, 60, 61]. Ligand
280 independent cell death signaling by TRAIL receptors involves their intracellular accumulation
281 and, similarly, TRAIL-R1 is detected within the ER and Golgi in PEL cells.

282 Additionally, our results were obtained without the use of ER/Golgi stress-inducing agents and
283 instead represent a constitutively active TRAIL-R1 death signaling process in robustly growing
284 cells. Importantly, PEL cells are of post-germinal center B cell origin and terminal B cell
285 differentiation is typically accompanied by a broad expansion and alteration of the ER and Golgi.
286 However, PEL cell lines typically lack B cell surface marker and immunoglobulin expression and
287 the status of the ER/Golgi in PEL cell lines has not been investigated in depth. Interestingly,
288 KSHV has been reported to activate the UPR and dampen its downstream transcriptional
289 response during lytic reactivation and ER stress has been shown to trigger KSHV reactivation in
290 latently infected cells[65, 66]. However, we did not detect colocalization of TRAIL-R1 with MPZ-
291 DelS63 in latently infected BCBL-1, as has been reported for TRAIL-R2 in the context of cell
292 death during the UPR in HCT116[62].

293 In addition to TRAIL-R1, our work has implicated several other ER/Golgi resident processes in
294 cFLIP dependency. High confidence hits in our cFLIP resistance screens included most genes
295 of the UFMylation pathway. Inactivation of UFM1 or DDRGK1 reduced TRAIL-R1 expression,

296 which is likely to explain their detection in our screens. Compared to ubiquitin, UFM1 modifies
297 only few proteins. The 60S ribosomal subunit RPL26 has been proposed as the primary UFM1
298 target, where UFM1 modification promotes the processing of translationally stalled polypeptides
299 at the ER[48, 49]. While we did not directly test the role of UFM1 or RPL26 in the translation of
300 TRAIL-R1, UFMylation of RPL26 may explain the requirement for UFM1/DDRGK1 for TRAIL-R1
301 expression. UFMylation is induced in response to cellular stressors, directing nascent peptides
302 to the ER for degradation[40, 48, 49, 67, 68] and, accordingly, disruption of UFMylation has been
303 reported to induce ER stress and increase cell death[67, 69, 70]. Of note, genes in the UFMylation
304 pathway do not score as essential in our original PEL screens and their essentiality within the
305 Cancer Dependency Map is mixed[7, 71]. Thus, it is plausible that UFMylation could similarly allow
306 translation of pro-apoptotic proteins, like TRAIL-R1, to proceed. A varied requirement for
307 UFMylation for cellular survival is further supported by findings that deletion of DDRGK1 in
308 mouse plasma cells did not result in increased cell death[72].

309 Like UFMylation, we observed that JAGN1 promotes expression of TRAIL-R1. While little is
310 known about this gene, JAGN1 has been shown to participate in the secretory pathway in
311 myeloid cells and antibody-producing B cells [51, 73]. As with UFMylation, JAGN1 is increased in
312 response to ER stress and its depletion has been linked to increased apoptosis in
313 granulocytes[51, 74]. Importantly, our PEL CRISPR screens and establishment of a JAGN1 KO cell
314 line suggest that JAGN1 is non-essential in PEL cells. Similarly, the Cancer Dependency Map
315 indicates that JAGN1 is not broadly required for cellular survival[7, 71].

316 Finally, our data suggest that chondroitin sulfate proteoglycan biosynthesis and CXCR4 are
317 involved in the ligand-independent activity of TRAIL-R1. Since inactivation of neither pathway
318 affected TRAIL-R1 expression or cause re-distribution of TRAIL-R1 to the cell surface, the exact
319 mechanism underlying their link to TRAIL-R1 signaling and cFLIP dependency remains unclear.
320 Interestingly, both CXCR4 and its primary ligand, CXCL12, have been identified as targets of

321 chondroitin sulfate moieties, although the roles of these modifications remain unclear[75, 76].
322 However, CXCL12 is not endogenously expressed in PEL cells and TRAIL-R1-dependent cell
323 death in PEL cells is not overcome by chemical CXCR4 inhibition. While there is a report of
324 CXCR4-induced apoptosis, but this process was independent of CASP8 and could not be
325 inhibited by MC159L, unlike the TRAIL-R1-dependent process that is inhibited by cFLIP in PEL
326 cells[77]. Recent work indicates that misfolded integral membrane proteins, such as MPZ, can act
327 as non-canonical ligands for TRAIL-R2 activity during ER stress-induced cell death[62]. Notably,
328 rhodopsin, a member of the 7-pass transmembrane protein family to which CXCR4 belongs,
329 also demonstrated this activity[62]. Future work should therefore test whether misfolding of
330 endogenous CXCR4 serves as a trigger of ligand-independent TRAIL-R1 signaling in PEL cells.

331 In sum, our data strongly support a role for TRAIL-R1 in incorporating multiple ER/Golgi-
332 associated signals in PEL cells into a constitutive, ligand-independent cell death process that
333 must be inhibited by cFLIP to allow for cellular viability.

334

335 **Materials and Methods**

336 **Cloning**

337 Sequences for oligonucleotides and synthetic DNA fragments can be found in Supplementary
338 Tables S5A and S5B. All new vectors were confirmed by Sanger sequencing (ACGT, Inc.).
339 pLenti SpBsmBI sgRNA Hygro (Addgene, 62205) constructs were cloned by ligating annealed
340 oligonucleotides specified in Table S5C with the BsmBI-digested vector [78].
341 For rescue experiments, human C-terminally 3X-FLAG tagged FLIP long and short isoforms and
342 KSHV vFLIP were ordered as codon-optimized dsDNA gene fragment blocks (Integrated DNA
343 Technologies). This initial codon optimization introduced resistance to cFLIP sg1, while cFLIP
344 sg2 resistance was introduced via two overlapping PCRs centered on the sg2 target site using

345 the synthetic gene fragment as a template (primers 4672/4673 and 4674/4323). PCR products
346 were then inserted between the AgeI and BamHI sites of vector pLC-IRES-HYG [64] using Gibson
347 assembly. KSHV vFLIP was cloned from a codon-optimized gene fragment block containing the
348 entire vCyclin/vFLIP locus using primers 4317/4318 and Gibson assembled with 3X-FLAG PCR
349 products amplified from the cFLIP-S gene fragment (primers 4319/4323). PCR products
350 containing MC159L (primers 4338/4339) and MC160L (primers 4340/4341) were amplified from
351 pBabe-based vectors kindly provided by Dr. Joanna Shisler (UIUC) and Gibson assembled with
352 3X-FLAG PCR products amplified from the cFLIP-S gene fragment (primers 4342/4323 for
353 MC159L or 4343/4323 for MC160L).
354 vCyc and vFLIP expression constructs for transfection into 293T in Fig. S1A were cloned into
355 pMSCVpuro (Takara, Catalog # 631461) by PCR, using primers 3646/3647 (vCyc) and
356 3648/3649 (vFLIP), followed by Gibson assembly with the EcoRI/XhoI digested vector.

357 LentiGuide-Puro expressing cFLIP sg2 was cloned by ligation of annealed oligos 4532/4533
358 with BsmBI-linearized vector as described [7].

359 The parental shR-miR expression vector pZIP-ZsGreen-T2A-Hyg-shNT4 was cloned by
360 replacing the EcoRI-IRES-PuroR-NotI cassette of shERWOOD-UltramiR Lentiviral shRNA NT
361 control #4 in pZIP-hCMV-ZsGreen-Puro (Transomic) with a PCR product containing a T2A-
362 HygR cassette that was amplified using primers 3551/3552 and template lenti MS2-P65-
363 HSF1_Hygro (Addgene Plasmid #61426). The initial control insert shRNA NT control #4 was
364 replaced by digesting pZIP-ZsGreen-T2A-Hyg-shNT4 with NotI and MluI and inserting miR-30-
365 based shRNAs for cFLIP (sh1, shM, shN) or negative control shRNAs targeting Renilla
366 Luciferase (Ren.308 and Ren.713) using Gibson Assembly. These shRNAs were designed
367 using SplashRNA and/or as previously published [79]. dsDNA fragments specified in Table S5
368 were ordered and used for Gibson Assembly, either directly (shM, N) or after PCR-amplification
369 with primers 4594/4607 (sh1, Ren.308, Ren.713).

370 To clone cFLIP sg1 for DOX-inducible gene inactivation (Fig. S7B, C), we replaced the
371 sgAAVS1 sequence within pLX-sgAAVS1[64] using overlap PCR. PCR fragment 1 was amplified
372 using the forward primer 2430 and the sgRNA-specific reverse primer 5313. PCR fragment 2
373 was amplified using the sgRNA-specific forward primer 5312 and reverse primer 2431.
374 Fragments 1 and 2 were joined using overlap PCR with primers 2430 and 2431, cut with XhoI
375 and NheI and ligated with XhoI/NheI-digested pLX-sgRNA vector using T4 DNA ligase.

376 To clone the parental DOX-inducible lentiviral vector pCW-MCS-Zeo, we used Gibson assembly
377 of a PCR fragment allowing for zeocin resistance (generated using primers 5327 and 5328) and
378 SbfI/BamHI-digested pCW-MCS-PGK-P2A[80]. To clone pCW-Zeo-mCherry, pCW-Zeo-MPZ-
379 S63Del-mCherry, and pCW-Zeo-MPZ-S63Del-EctoYtoE-mCherry, we performed Gibson
380 Assembly of the AgeI-MluI vector fragment of pCW-MCS-Zeo with a PCR product containing
381 mCherry (primers 5320/5321), gBlocks 5324 and 5322 (DelS63), or gBlocks 5326 and 5322
382 (DelS63/EctoYtoE).

383 **Western blotting**

384 Cells were pelleted, washed in ice-cold PBS, in some cases stored at -80°C, and lysed for 30
385 minutes in ice-cold RIPA buffer containing 1X protease inhibitor cocktail (Sigma-Aldrich, catalog
386 P8340). Lysates were then subjected to five cycles (30 seconds on/30 seconds off) of
387 sonication at 4°C on high intensity in a Bioruptor Sonication System (Diagenode) and
388 subsequently cleared by centrifugation at 14,000g for 15 minutes. Lysates were diluted 5- to 10-
389 fold and quantified by Pierce BCA Protein Assay (ThermoFisher Scientific, 23225). Lysates
390 were denatured by heating at 70°C for 10 minutes in 1X LDS buffer (ThermoFisher, NP0008)
391 containing a final concentration of 2.5% beta-mercaptoethanol and loaded onto Bolt 4-12% Bis-
392 Tris gels (ThermoFisher Scientific; NW0412) at equivalent concentrations (15-20 µg for cFLIP
393 knockout validation based on available lysates; 50 µg for vCyc/vFLIP, and 20-30 µg for all other

394 proteins). SDS-PAGE was performed in 1X MES buffer and proteins were transferred onto
395 0.2 µm nitrocellulose membranes (Bio-Rad, 1620112).
396 Membranes were blocked at room temperature for 1 hour and probed overnight at 4 °C with
397 primary antibodies at the concentrations indicated in Table S5D. Images were captured on an
398 Odyssey FC (LI-COR Biosciences) after incubation with IRDye 800CW secondary antibodies
399 (LI-COR Biosciences) at a 1:15000 concentration. In some cases, anti-rat HRP (Santa Cruz) at
400 a 1:5000 concentration was used for detection and developed using SuperSignal West Femto
401 Maximum Sensitivity Substrate (ThermoFisher Scientific, 34094) following manufacturer
402 protocol. Contrast/brightness was dynamically adjusted as needed using ImageStudio. Bands
403 were quantified in ImageStudio Lite version 5.2 (LI-COR Biosciences). Original Western Data
404 are included as one supplemental file.

405 **Cell culture**

406 PEL and/or BJAB cell lines were maintained in RPMI 1640 with L-glutamine (Corning,
407 MT10040CM) supplemented with 10% (BC-1, BCBL-1) or 20% (BC-2, BC-3, BC-5, BJAB)
408 Serum Plus-II (Sigma-Aldrich, catalog number 14009C, lots 15H243 and 21C421), 10 µg/mL
409 gentamycin (ThermoFisher Scientific, 15710064) and 0.05 mM beta-mercaptoethanol (Sigma-
410 Aldrich, M3148-25ML). HEK293T cells were maintained in DMEM (Sigma-Aldrich, D5796)
411 supplemented with 10% Serum Plus-II and 10 mg/mL gentamycin. PEL cells were counted by
412 trypan exclusion and split every second day to approximately $2x10^5$ cells/mL (or $3x10^5$ for BC-
413 5). 293T cells were maintained at visually sub-confluent densities and split every 2 days. PEL
414 cell lines expressing lentiCas9-Blast (Addgene, 52962) were previously generated and validated
415 by STR profiling[7]. The BC-1/Cas9 clonal cell line utilized in Fig. 1B was subcloned and selected
416 for editing efficiency compared to the parental Cas9 BC-1 pool utilized in the screens. This BC-
417 1/Cas9 clone was re-confirmed by STR profiling. A stable BCBL-1 cell clone allowing for DOX-
418 inducible Cas9 expression (BCBL-1/pCW-Cas9) was reported previously[64].

419 For cellular growth curves and functional titration of lentivirus other than pZIP-based vectors
420 (see below), cells were counted by flow cytometry using spike-in of a known amount of
421 AccuCount Blank Particles 5-5.9 µm (Spherotech, ACBP-50-10) as previously described[7].

422 **Cumulative cellular growth curves**

423 Importantly, all lentiviral vectors used for growth curves analyses were titrated in naïve parental
424 cell lines to ensure comparable titers between control sgRNAs and toxic sgRNAs. For growth
425 curves, cells were plated at a density of $3x10^5$ cells/mL and transduced at the multiplicities of
426 infection (MOIs) indicated in the text or figure legends. Medium was exchanged one day after
427 transduction and cells were selected with 1.2 µg/mL puromycin for 2 days; 200 µg/mL
428 hygromycin for 3 days (titrations) or 5-7 days (stable cell line production). Every second day,
429 cells were counted by flow cytometry as described above and then split to a density of $2x10^5$
430 cells/mL. This process was repeated until cells that had received toxic sgRNAs were too sparse
431 to split or for up to 10 days. Cumulative cell counts were calculated by taking the measured cell
432 concentration at a given timepoint multiplied by the product of all previous dilution factors and
433 normalized to cumulative cell counts obtained for the sgAAVS1 control.

434 Statistical testing for reduced cellular viability was performed using one-sided, one-sample t-
435 testing (H_0: $P(\mu=1)$ with H_A: $P(\mu<1)$). For rescue growth curve experiments (i.e. in the context of
436 ectopic FLIP expression or a knockout cell pool) an additional one-sided, independent two-
437 sample t-test was performed, comparing the relative cumulative cell counts for each guide
438 between the experimental cell line and the control line (i.e. sgAAVS1-Hygro or ZsGreen-Hygro).
439 In the case of ZsGreen or KSHV vFLIP expression for rescue experiments, where n= 3-6 were
440 obtained for up to day 10 (Fig. 2C), ordinary least squares regression lines were fit. Cumulative
441 cell counts relative to cell-line matched sgAAVS1 were used as the singular dependent variable
442 with one or two predictor variables. To measure depletion, data was subset on the indicated cell
443 line (ZsGreen or vFLIP expression) and sgRNA (sgPSM1 or cFLIP sg1) with the timepoint (>0

444 days after transduction) as a singular predictor variable. To measure rescue, data was subset
445 on a particular sgRNA (sgPSMD1 or cFLIP sg1) with the cell line (ZsGreen or vFLIP) as an
446 additional categorical predictor variable besides the timepoint (2-8 days post-transduction). A
447 one-sided t-test was then used to determine whether the coefficients for day (depletion) or cell
448 line (rescue) were < or > 0, respectively.

449 **Lentiviral production, infection, and titration**

450 Except for pZIP-based vectors, lentivirus was produced using packaging plasmids psPAX2,
451 pMD2.G, and transfer vectors at 1.3:0.72:1.64 molar ratios. HEK293T Cells were seeded at a
452 density of 1.25×10^7 per 15-cm dish and transfected with 30 µg of DNA using a 1:3 to 1:3.5 ratio
453 of µg of DNA to µL PEI. Media were replaced after ~6 hours and cell supernatants containing
454 viral vectors were collected 48-72 hours later and filtered through 450nm pore size filters. Viral
455 vector preparations were used as is or concentrated by ultracentrifugation or using Amicon Ultra
456 Centrifugal Filter Units (Millipore, UFC910024) following manufacturer protocol. In some cases,
457 lentivirus was stored at -80°C.

458 Lentiviral vector titers were measured using functional titration of serially diluted viral stocks.
459 The multiplicity of infection (MOI) of each dilution point was estimated using the percentage of
460 live cells relative to an untreated control and a resulting viral concentration (transducing
461 units/mL) was calculated from the average of multiple dilution points assuming a Poisson
462 distribution, $P(x) = \frac{\lambda^x e^{-\lambda x}}{x!}$, to estimate the mean event rate λ (MOI) assuming P(x=0) is the
463 percentage of uninfected cells.

464 Transductions were carried out at 3×10^5 cells/mL and the indicated MOIs under normal culture
465 conditions supplemented with 5 µg/mL polybrene (Sigma-Aldrich, TR-1003-G). Culture medium
466 was replaced ~24 hours after transduction and antibiotic resistance selection was carried out

467 using 1.2 µg/mL puromycin for 2 days; 200 µg/mL hygromycin for 3 days (titrations) or 5-7 days
468 (stable cell line production and CRISPR screens).

469 Procedures for pZIP-ZsGreen-T2A-Hygro shRNA vectors are described below.

470 **CRISPR-based single-gene knockout**

471 CRISPR knockout was achieved by transduction of published Cas9-expressing cell pools or
472 clones and published lentiviral single guide RNA constructs for AAVS1, PSMD1 sg1, IRF4 sg1,
473 cFLIP sg1. A new cFLIP sg2 was cloned for this paper since sg2 from the previous study
474 performed sub-optimally. The new cFLIP sg2 corresponds to sgRNA 2 (by rule set 2 score, on
475 target activity) from the Brunello library. sgRNAs in pLentiGuide-Puro (Addgene, 52963) were
476 used for cumulative growth curve knockout, while long-term single-gene knockout cell lines
477 were generated using sgRNAs in pLenti SpBsmBI sgRNA Hygro (Addgene, 62205) containing a
478 hygromycin resistance cassette. Sequences of all sgRNAs can be found in Table S5C.

479 **CRISPR-based synthetic rescue screens with sgRNA challenge**

480 Library virus was generated and titrated as described above using the Brunello sgRNA pool
481 library in lentiGuide-Puro (Addgene, 73178). In all cases, approximately $9.2x10^7$ to $1.5x10^8$ cells
482 were transduced at an MOI of 0.3 to result in a single sgRNA per cell at a coverage of 300-500X
483 cells per guide. Transduced cells were selected using 1.2 µg/mL puromycin, and dropout was
484 allowed to proceed for 12 days with at least $3.6x10^7$ cells maintained to preserve library
485 complexity.

486 The resulting cell pool was then challenged with either cFLIP sg1 or the negative control
487 sgAAVS1 in pLenti SpBsmBI sgRNA Hygro at an MOI < 0.5. Cells were selected with
488 hygromycin and cultured until resistance to cFLIP knockout was apparent by cellular
489 proliferation, i.e. until day 12 after sgRNA transduction. At this point, approximately $3\text{-}7x10^8$ cells
490 (500-1000X coverage) were harvested, washed in ice-cold PBS, and snap frozen.

491 **shRNA-based synthetic rescue screens**

492 pZIP transfer vectors were packaged in Lenti-X 293T cells (Takara) using molar ratios of 0.2
493 transfer vector to 0.51 psPax2 to 0.29 pMD2.G. Briefly, $2.1x10^7$ pLenti-X 293T cells/15 cm dish
494 were transfected with ~48.5 µg total plasmid and supernatant was harvested 48 hours later
495 without replacing media. Supernatants were filtered through 450nm pore size filters and
496 concentrated by ultracentrifugation (Beckman SW32Ti, 25,000 rpm, 90 min), resuspend in
497 OptiMEM on a platform shaker for at least 60 min at 4°C and followed by pipetting up and down
498 20 times, aliquoted, and snap frozen at -80°C. Virus aliquots were thawed at 37°C and cleared
499 by centrifugation at 400 g for 5 min before use. Titration of the negative control vectors was
500 performed based on ZsGreen expression and flow cytometry in BCBL-1/Cas9 clone C2.
501 Titration of the toxic cFLIP shRNAs was performed in 293T cells lacking Dicer (293T/NoDice) [81],
502 relative to a negative control with known titer in BCBL-1/Cas9.

503 BCBL-1/Cas9 Brunello library transduction was performed at MOI 0.3 in eleven 15 cm dishes at
504 $5x10^5$ cells/mL and 50mL/dish, ~920x theoretical sgRNA coverage. Cells were selected using
505 1.2 µg/mL puromycin from days 1 to 4 after transduction and expanded. On Day 9 after Brunello
506 transduction, seven 15 cm dishes of cells ($3x10^5$ cells/mL and 50 mL/dish) were challenged with
507 each shRNA vector at MOI 0.5. The next day, cells were collected by centrifugation and
508 resuspended in fresh medium containing 200 µg/mL Hygromycin. Cell pools were maintained at
509 coverage and optimal cell density with hygromycin for one week and at least $4x10^7$
510 cells/condition were harvested on day 12 into the shRNA challenge.

511 **CRISPR library preparation and next-generation sequencing**

512 Genomic DNA was isolated following a previously described protocol and library preparation
513 was performed as previously described for sgRNA and shRNA screens in BCBL-1 [7]. Resulting
514 libraries were quantified by Qubit (ThermoFisher Scientific, Q33231) prior to further QC and

515 quantification by Bioanalyzer (Agilent) and Kapa qPCR (Roche). Multiplexing of sgRNA
516 challenge screens in BCBL-1 was performed utilizing 6-bp indexes and sequenced on a single
517 lane of a HiSeq4000 (Illumina) using 50bp single-end (SE) reads with 10% PhiX spike-in as
518 previously described[7]. For sgRNA challenge screens in BC-2, sequencing was performed on a
519 single flow-cell of an NextSeq 500 (Illumina) using 75bp SE reads with 10% PhiX spike-in due to
520 the discontinuation of the HiSeq4000 platform. For these runs, library preparation was modified
521 slightly to combine genomic amplification and addition of adapters/barcode into a single PCR
522 step with custom 8bp indexes (sequences can be found in Table S5E). The shRNA-based
523 screens were prepped and sequenced twice as a quality control using both
524 approaches/platforms and reads were subsequently merged for further analysis. Demultiplexed
525 reads have been deposited on GEO (accession GSE210445).

526 5' adapters were trimmed from raw CRISPR sequencing reads and trimmed to length (20 bp)
527 from the 3' end using Cutadapt v4.1 [82]. Reads were then aligned using Bowtie v1.1.2 9 [83].
528 Guide-level counts were obtained using MAGeCK v0.5.9 and statistical testing was performed
529 using MAGeCK's robust rank aggregation (RRA) algorithm using median normalization [84].

530 **CRISPR Knockout Pools Indel Sequencing**

531 A 200-300 bp region around each indicated guide was amplified from genomic DNA using the
532 primers indicated in Table S5F and sent to Massachusetts General Hospital CCIB DNA Core for
533 low depth sequencing. Raw FASTQ files were assembled into contigs by MGH and the resulting
534 effect on the coding sequence was determined using custom alignment and classification script
535 built using Biopython [85] to estimate indel, frameshift, and early stopping incidence. Briefly,
536 assembled contigs were aligned to the coding sequences targeted by each amplicon to
537 determine optimal positioning of the contig in reference to the full coding sequence. All
538 alignments utilized a simple pairwise scoring matrix (+1 for matches, +0 for mismatches, -.99 for
539 gap opening, and -0 for gap extensions) chosen by iterative manual assessment of the

540 collective results for the most abundant contig for each gene. The resulting, fully assembled
541 coding sequence was then classified as an indel or non-indel for all sequences. Indels were
542 further characterized as in-frame or frameshifted based on the number of nucleotides lost or
543 gained across all alignment gaps. Early stopping events for all variants were predicted by *in*
544 *silico* translation of predicting coding sequences. Raw FASTQ output was also analyzed using
545 CRISPResso2[86] to obtain estimates of the number of modified and frameshifted reads.

546 **mRNA Sequencing**

547 A frozen BC-1 lysate in Trizol was submitted to BGI Group (Shenzhen, China) for single-ended,
548 polyA-enriched RNA sequencing. Un-trimmed reads were aligned to the Gencode 41 annotation
549 of GRCh38.p13 with STAR v2.7.10. Raw sequencing data has been made available on GEO
550 (accession GSE210446).

551 **RNA Purification and Reverse Transcription**

552 $5x10^6$ Cells were washed in ice-cold PBS, pelleted, and resuspended in 300 uL TRIzol
553 (Invitrogen, 15596026). RNA was isolated using the Zymo Research Direct-zol RNA Miniprep
554 Kit (Fisher Scientific, NC1057004) following the manufacturer's protocol. Purified RNA was
555 treated with RQ1 RNAse-free DNAse (Promega, M6101) using 1 µL DNase per 5 µL RNA in a
556 final volume of 10 µL volume. Poly-dT primed reverse transcription was performed using the
557 SuperScript First-Strand Synthesis System (Invitrogen, 11904018) using 1 µg of RNA as
558 template in a 10 µL reaction, including water-only reactions as non-template controls, following
559 manufacturer protocols including optional RNAse digestion after reverse transcription. Samples
560 were then diluted to 100 ng calculated input RNA/4.5 µL prior to TaqMan assay.

561 **TaqMan Assay**

562 Real-time PCR was performed by standard TaqMan Assay on either the QuantStudio 7 or
563 Quantstudio 5 Real-Time PCR platform (Applied Biosystems). Briefly, a mastermix of 1 µL

564 TaqMan probe (Applied Biosystems, Hs00269492_m1 or Hs00984230_m1) to 10 µL TaqMan
565 Universal Master Mix II (Applied Biosystems, 4440043) was prepared for each probe. 5.5 µL of
566 mastermix was added per well, followed by 4.5 µL (equivalent to 100 ng calculated input RNA)
567 cDNA template. Three technical replicates were included, and $2^{-\Delta\Delta CT}$ was calculated relative to
568 the endogenous B2M control and sgAAVS1-transduced cell line for each biological replicate[87].
569 Biological replicates represent independently harvested cell pellets of the indicated cell lines.
570 Statistical testing for differences between samples was performed using one-way analysis of
571 variance. Post-hoc testing was performed using Dunnett's method and sgAAVS1 as the control
572 group.

573 **Inducible CRISPR/Cas9 Assay and AMD3100 Treatment**

574 For data shown in Fig. 7B-C, we transduced BCBL-1 with stably integrated DOX-inducible Cas9
575 (BCBL-1/pCW-Cas9[64]) with pLX-sgRNA-lentiviral vectors expressing sgRNAs targeting AAVS1,
576 PSMD1, or cFLIP sg1 at ~MOI 2 and selected transduced cells with 7.5 µg/ml Blasticidin S
577 (Sigma-Aldrich, SBR00022). We induced Cas 9 expression by treatment with 1 µg/ml
578 Doxycycline hyclate (DOX, Sigma-Aldrich, D9891-1G) or left the cultures uninduced. At the
579 same time, we further treated each cell line and DOX-treatment group with DMSO or 25 µM
580 AMD3100 (Selleckchem, S8030). Cells were counted by trypan exclusion every 2-3 days,
581 pelleted, and re-suspended to $2x10^5$ cells/mL in fresh medium containing the specified drugs.

582 **Cellular staining and flow cytometry**

583 Cells were washed twice in ice-cold PBS and APC Annexin V (BD Biosciences, 550475) and 7-
584 AAD (BD Biosciences, 559925) staining was performed on $1x10^5$ cells in 100 µL of 1X Annexin
585 V binding buffer (BD Biosciences, 556454) following manufacturer recommended guidelines,
586 using 5 µL of each stain for 15 minutes at room temperature in the dark. Necrotic cells were
587 generated for Annexin V and 7-AAD compensation controls using a 30-minute heat shock at

588 95°C. Stained cells were diluted with 400 µL 1x Annexin V binding buffer and flow cytometry
589 was performed on a BD FACSCanto II (BD Biosciences) within 1 hour.

590 For TRAIL-R1 staining, cells were harvested and washed twice in ice-cold PBS and
591 resuspended in PBS at a concentration of $1x10^6$ cells/mL. 500 µL of cells were then fixed in
592 PBS containing 4% w/v formaldehyde (FA, ThermoFisher Scientific, PI28908) for 10 minutes
593 followed by two more PBS washes. On the final wash, cells were split into two and each
594 resuspended in 250 µL PBS containing 1% w/v bovine serum albumin (BSA, Sigma,
595 10735078001) with or without the addition of 0.1% w/v saponin (Sigma-Aldrich, 47036). Cells
596 were pre-incubated for 15 minutes at room temperature with 250 µL PBS/1% BSA with or
597 without 0.1% w/v saponin, containing 1:400 of Human BD Fc Block (ThermoFisher Scientific,
598 BDB564219) per condition, followed by addition of 1:100 (2.5 µL in 250 µL) of FITC-conjugated
599 anti-TRAIL receptor 1 (Abcam, ab59047; specific to the extracellular domain of TRAIL-R1) for
600 30 minutes at room temperature in the dark. Cells were then washed 3X with PBS/1% BSA with
601 or without 0.1% w/v saponin followed by a final re-suspension in 500 µL PBS containing 0.01%
602 FA.

603 Stained cells were stored for up to 2 days at 4°C in the dark (TRAIL-R1) and flow cytometry was
604 performed on a BD FACSCanto II (BD Biosciences). Raw data were exported to FlowJo v10.8.1
605 for analysis and plotting.

606 **BCBL-1 cell lines expressing MPZ-Del63-mCherry constructs**

607 To allow for inducible expression of mCherry, MPZ-Del63-mCherry, or MPZ-DelS63-EctoYtoE-
608 mCherry, we transduced naïve BCBL-1 cells at MOI <1. We selected transduced cells with 175
609 µg/ml zeocin (Life Technologies, R25005) and induced protein expression by treatment with 1
610 µg/ml DOX. Results in Figs. 5E-F and S5D-E are from day 3 after induction and three
611 independent inductions.

612 **Immunofluorescence and colocalization analysis**

613 Cells were collected by centrifugation, washed with PBS, and resuspended in PBS at $1x10^6$
614 cells/mL. 650 µL/24 well or 3ml/6 well were spun onto 1.5mm thick, uncoated glass coverslips in
615 swing bucket rotors at 650 g for 5 minutes. Coverslips were fixed for 15 minutes with 4%
616 formaldehyde (FA)–PBS, rinsed three times with PBS, and blocked for 1 hour in PBS containing
617 0.1% w/v saponin-3% bovine serum albumin (BSA, Sigma Aldrich, A7906). Samples were again
618 rinsed three times with PBS and incubated with primary antibodies as indicated in Table S5D,
619 diluted in PBS containing 0.1% w/v saponin-3% BSA for 1 hour at 37°C in a humidified
620 chamber. Coverslips were rinsed three times and incubated with the appropriate species IgG
621 (H+L) highly cross-adsorbed secondary antibody conjugated to Alexa Fluor 488 (TRAIL-R1
622 staining) or 568 (all others) diluted 1:1000 in PBS containing 0.1% w/v saponin-3% BSA for
623 1 hour at 37°C in a humidified chamber. Coverslips were washed with PBS, incubated with 4′,6-
624 diamidino-2-phenylindole (DAPI) as directed (Invitrogen, D1306), and washed with PBS. Finally,
625 coverslips were mounted onto glass slides using ProLong Gold antifade mountant (Invitrogen,
626 P36934), and incubated at room temperature in the dark for 24 hours.

627 Confocal images were acquired on a Nikon W1 Dual Cam Spinning Disk Confocal microscope
628 with Plan Apo λ 60x Oil objective. Widefield images were acquired in Z-stacks on a Nikon Ti-2
629 Widefield microscope with S Plan Fluor ELWD 40x Ph2 ADM air objective and analyzed with
630 Imaris software for 3D colocalization of the top 10% brightest voxels per channel.

631 **Enzyme-linked immunosorbent assay**

632 Anti-TRAIL ELISA was performed using a Human TRAIL/TNFSF10 Quantikine ELISA Kit (R&D
633 Systems, DTRL00) following manufacturer-provided protocols. Briefly, 50 µL of cell supernatant
634 or cellular lysate obtained using manufacturer provided buffers and instructions were added to
635 each well. Cell densities at time of harvesting were $8x10^6$ to $1.2x10^7$ PEL cells, while cells were

636 lysed at a concentration of $1x10^7$ cells/mL as per manufacturer guidelines. The included
637 recombinant human TRAIL standard (R&D Systems, 892375) was serially diluted in 2-fold steps
638 from 1000 to 15.6 pg/mL. Absorbance was read on a VICTOR Nivo Plate reader at 450 nm. A
639 blank measurement taken from a well containing clean dilution buffer was subtracted from all
640 other wells and least squares regression was performed on the measured values across all
641 replicates to determine effective concentrations.

642 **In vitro TRAIL treatment**

643 BCBL-1/Cas9 cells containing pLenti SpBsmBI Guide Hygro (AAVS1 or TRAIL-R1 #1/2) were
644 treated with the indicated serial dilutions of recombinant human TRAIL (Sigma-Aldrich, T9701)
645 and absolute cell numbers were measured 24 hours later by flow cytometry as described above
646 for cumulative growth curves.

647 **Statistical Analysis**

648 Statistical testing/modeling was conducted in Python using SciPy 1.6.0[88] (simple t tests, one-
649 way ANOVA) or Statsmodels 0.13.2 (ordinary least squares) unless otherwise indicated.
650 Vertical bar graphs were generated using Prism 9.4.1 (GraphPad), all other figures were
651 generated using Seaborn 0.11.2 [89]. For groups of tests with similar hypotheses, i.e. similar
652 comparisons in the same figure panel, false-discovery adjusted p-values were calculated using
653 the Benjamini-Hochberg procedure implemented in Statsmodels. For two-sample t-tests, equal
654 variances were assumed. Specific tests are indicated in the figure legends. Full code for
655 computational and statistical analyses was made available online on Github
656 (https://github.com/Gottwein-Lab).

657 **Acknowledgements**

658 We would like to thank Dr. Joanna Shisler for sharing MCV FLIP protein expression vectors and
659 Dr. Ethel Cesarman for sharing a control aliquot of BC-3 cells. Imaging work was performed at

660 the Northwestern University Center for Advanced Microscopy generously supported by NCI
661 CCSG P30 CA060553 awarded to the Robert H Lurie Comprehensive Cancer Center.

662 **Competing Interests** The authors do not have competing interests.

663 **Author Contributions** Study Design NK, SO, MM and EG. MM performed exploratory
664 resistance screens in BC-3, which were not included in the final manuscript due to very low
665 cFLIP dependency of this cell line. NK performed most experiments. EG performed shRNA
666 cloning, pLX and pCW cell line construction, and shRNA resistance screens until harvest of cell
667 pellets. SMO performed all immunofluorescence staining and analyses. ZL performed pLX and
668 pCW vector cloning. Computational and statistical analyses were performed by NK. NK and SO
669 put together figures, which were edited by EG. NK, SO, and EG wrote the manuscript. EG
670 supervised all aspects of the work. All authors read and approved the final manuscript.

671 **Ethics Statement** This study did not require ethical approval.

672 **Funding** This work was supported by NCI R01 CA247619 and R01 CA247619-01A1S1 to E.G.;
673 MM was supported by K22 CA241355.

674 **Data Availability** CRISPR screening and RNAseq data were deposited on GEO (accessions
675 GSE210445, GSE210446). All cell lines and plasmids are available on request.

676

677 **References**

678

679 1. Cesarman E, Chang Y, Moore PS, Said JW, Knowles DM. Kaposi's sarcoma-associated
680 herpesvirus-like DNA sequences in AIDS-related body-cavity-based lymphomas. *N Engl*
681 *J Med* 1995, **332**(18)**:** 1186-1191.

682

683 2. Nador RG, Cesarman E, Chadburn A, Dawson DB, Ansari MQ, Sald J*, et al.* Primary
684 effusion lymphoma: a distinct clinicopathologic entity associated with the Kaposi's
685 sarcoma-associated herpes virus. *Blood* 1996, **88**(2)**:** 645-656.

686

687 3. Lurain K, Polizzotto MN, Aleman K, Bhutani M, Wyvill KM, Goncalves PH*, et al.* Viral,
688 immunologic, and clinical features of primary effusion lymphoma. *Blood* 2019, **133**(16)**:**
689 1753-1761.

690

691 4. Wies E, Mori Y, Hahn A, Kremmer E, Sturzl M, Fleckenstein B*, et al.* The viral interferon-
692 regulatory factor-3 is required for the survival of KSHV-infected primary effusion
693 lymphoma cells. *Blood* 2008, **111**(1)**:** 320-327.

694

695 5. Godfrey A, Anderson J, Papanastasiou A, Takeuchi Y, Boshoff C. Inhibiting primary
696 effusion lymphoma by lentiviral vectors encoding short hairpin RNA. *Blood* 2005, **105**(6)**:**
697 2510-2518.

698

699 6. Chaudhary PM, Jasmin A, Eby MT, Hood L. Modulation of the NF-kappa B pathway by
700 virally encoded death effector domains-containing proteins. *Oncogene* 1999, **18**(42)**:**
701 5738-5746.

702

703 7. Manzano M, Patil A, Waldrop A, Dave SS, Behdad A, Gottwein E. Gene essentiality
704 landscape and druggable oncogenic dependencies in herpesviral primary effusion
705 lymphoma. *Nat Commun* 2018, **9**(1)**:** 3263.

706

707 8. Hu S, Vincenz C, Buller M, Dixit VM. A novel family of viral death effector domain-
708 containing molecules that inhibit both CD-95- and tumor necrosis factor receptor-1-
709 induced apoptosis. *J Biol Chem* 1997, **272**(15)**:** 9621-9624.

710

711 9. Irmler M, Thome M, Hahne M, Schneider P, Hofmann K, Steiner V*, et al.* Inhibition of
712 death receptor signals by cellular FLIP. *Nature* 1997, **388**(6638)**:** 190-195.

713

714 10. Thome M, Schneider P, Hofmann K, Fickenscher H, Meinl E, Neipel F*, et al.* Viral
715 FLICE-inhibitory proteins (FLIPs) prevent apoptosis induced by death receptors. *Nature*
716 1997, **386**(6624)**:** 517-521.

717

718 11. Krueger A, Schmitz I, Baumann S, Krammer PH, Kirchhoff S. Cellular FLICE-inhibitory
719 protein splice variants inhibit different steps of caspase-8 activation at the CD95 death-
720 inducing signaling complex. *J Biol Chem* 2001, **276**(23)**:** 20633-20640.

721

722 12. Kataoka T, Budd RC, Holler N, Thome M, Martinon F, Irmler M*, et al.* The caspase-8
723 inhibitor FLIP promotes activation of NF-kappaB and Erk signaling pathways. *Curr Biol*
724 2000, **10**(11)**:** 640-648.

725

726 13. Chugh P, Matta H, Schamus S, Zachariah S, Kumar A, Richardson JA*, et al.*
727 Constitutive NF-κB activation, normal Fas-induced apoptosis, and increased incidence of
728 lymphoma in human herpes virus 8 K13 transgenic mice. *Proceedings of the National*
729 *Academy of Sciences of the United States of America* 2005, **102**(36)**:** 12885-12890.

730

731 14. Bélanger C, Gravel A, Tomoiu A, Janelle ME, Gosselin J, Tremblay MJ*, et al.* Human
732 herpesvirus 8 viral FLICE-inhibitory protein inhibits Fas-mediated apoptosis through
733 binding and prevention of procaspase-8 maturation. *J Hum Virol* 2001, **4**(2)**:** 62-73.

734

735 15. Tolani B, Matta H, Gopalakrishnan R, Punj V, Chaudhary PM. NEMO is essential for
736 Kaposi's sarcoma-associated herpesvirus-encoded vFLIP K13-induced gene expression
737 and protection against death receptor-induced cell death, and its N-terminal 251
738 residues are sufficient for this process. *J Virol* 2014, **88**(11)**:** 6345-6354.

739

740 16. Galluzzi L, Vitale I, Aaronson SA, Abrams JM, Adam D, Agostinis P*, et al.* Molecular
741 mechanisms of cell death: recommendations of the Nomenclature Committee on Cell
742 Death 2018. *Cell Death & Differentiation* 2018, **25**(3)**:** 486-541.

743

744 17. Fritsch M, Gunther SD, Schwarzer R, Albert MC, Schorn F, Werthenbach JP*, et al.*
745 Caspase-8 is the molecular switch for apoptosis, necroptosis and pyroptosis. *Nature*
746 2019, **575**(7784)**:** 683-687.

747

748 18. Newton K, Wickliffe KE, Maltzman A, Dugger DL, Reja R, Zhang Y*, et al.* Activity of
749 caspase-8 determines plasticity between cell death pathways. *Nature* 2019, **575**(7784)**:**
750 679-682.

751

752 19. Yu L, Alva A, Su H, Dutt P, Freundt E, Welsh S*, et al.* Regulation of an ATG7-beclin 1
753 program of autophagic cell death by caspase-8. *Science* 2004, **304**(5676)**:** 1500-1502.

754

755 20. Bell BD, Leverrier S, Weist BM, Newton RH, Arechiga AF, Luhrs KA*, et al.* FADD and
756 caspase-8 control the outcome of autophagic signaling in proliferating T cells. *Proc Natl*
757 *Acad Sci U S A* 2008, **105**(43)**:** 16677-16682.

758

759 21. Jimbo A, Fujita E, Kouroku Y, Ohnishi J, Inohara N, Kuida K*, et al.* ER stress induces
760 caspase-8 activation, stimulating cytochrome c release and caspase-9 activation. *Exp*
761 *Cell Res* 2003, **283**(2)**:** 156-166.

762

763 22. Munoz-Pinedo C, Lopez-Rivas A. A role for caspase-8 and TRAIL-R2/DR5 in ER-stress-
764 induced apoptosis. *Cell Death Differ* 2018, **25**(1)**:** 226.

765

766 23. Grundhoff A, Ganem D. Mechanisms governing expression of the v-FLIP gene of
767 Kaposi's sarcoma-associated herpesvirus. *J Virol* 2001, **75**(4)**:** 1857-1863.

768

769 24. Liu L, Eby MT, Rathore N, Sinha SK, Kumar A, Chaudhary PM. The human herpes virus
770 8-encoded viral FLICE inhibitory protein physically associates with and persistently
771 activates the Ikappa B kinase complex. *J Biol Chem* 2002, **277**(16)**:** 13745-13751.

772

773 25. Field N, Low W, Daniels M, Howell S, Daviet L, Boshoff C*, et al.* KSHV vFLIP binds to
774 IKK-gamma to activate IKK. *J Cell Sci* 2003, **116**(Pt 18)**:** 3721-3728.

775

776 26. Sun Q, Matta H, Chaudhary PM. The human herpes virus 8-encoded viral FLICE
777 inhibitory protein protects against growth factor withdrawal-induced apoptosis via NF-
778 kappa B activation. *Blood* 2003, **101**(5)**:** 1956-1961.

779

780 27. Bagneris C, Rogala KB, Baratchian M, Zamfir V, Kunze MB, Dagless S*, et al.* Probing
781 the Solution Structure of IkappaB Kinase (IKK) Subunit gamma and Its Interaction with
782 Kaposi Sarcoma-associated Herpes Virus Flice-interacting Protein and IKK Subunit beta
783 by EPR Spectroscopy. *J Biol Chem* 2015, **290**(27)**:** 16539-16549.

784

785 28. Hu WH, Johnson H, Shu HB. Activation of NF-kappaB by FADD, Casper, and caspase-
786 8. *J Biol Chem* 2000, **275**(15)**:** 10838-10844.

787

788 29. Kataoka T, Tschopp J. N-terminal fragment of c-FLIP(L) processed by caspase 8
789 specifically interacts with TRAF2 and induces activation of the NF-kappaB signaling
790 pathway. *Mol Cell Biol* 2004, **24**(7)**:** 2627-2636.

791

792 30. Baratchian M, Davis CA, Shimizu A, Escors D, Bagneris C, Barrett T*, et al.* Distinct
793 Activation Mechanisms of NF-kappaB Regulator Inhibitor of NF-kappaB Kinase (IKK) by
794 Isoforms of the Cell Death Regulator Cellular FLICE-like Inhibitory Protein (cFLIP). *J Biol*
795 *Chem* 2016, **291**(14)**:** 7608-7620.

796

797 31. Shisler JL, Moss B. Molluscum contagiosum virus inhibitors of apoptosis: The MC159 v-
798 FLIP protein blocks Fas-induced activation of procaspases and degradation of the
799 related MC160 protein. *Virology* 2001, **282**(1)**:** 14-25.

800

801 32. Nichols DB, Shisler JL. The MC160 protein expressed by the dermatotropic poxvirus
802 molluscum contagiosum virus prevents tumor necrosis factor alpha-induced NF-kappaB
803 activation via inhibition of I kappa kinase complex formation. *J Virol* 2006, **80**(2)**:** 578-
804 586.

805

806 33. Biswas S, Smith GL, Roy EJ, Ward B, Shisler JL. A comparison of the effect of
807 molluscum contagiosum virus MC159 and MC160 proteins on vaccinia virus virulence in
808 intranasal and intradermal infection routes. *J Gen Virol* 2018, **99**(2)**:** 246-252.

809

810 34. Ma Y, Walsh MJ, Bernhardt K, Ashbaugh CW, Trudeau SJ, Ashbaugh IY*, et al.*
811 CRISPR/Cas9 Screens Reveal Epstein-Barr Virus-Transformed B Cell Host
812 Dependency Factors. *Cell Host Microbe* 2017, **21**(5)**:** 580-591.e587.

813

814 35. Doench JG, Fusi N, Sullender M, Hegde M, Vaimberg EW, Donovan KF*, et al.*
815 Optimized sgRNA design to maximize activity and minimize off-target effects of
816 CRISPR-Cas9. *Nat Biotechnol* 2016, **34**(2)**:** 184-191.

817

818 36. Sherman BT, Hao M, Qiu J, Jiao X, Baseler MW, Lane HC*, et al.* DAVID: a web server
819 for functional enrichment analysis and functional annotation of gene lists (2021 update).
820 *Nucleic Acids Res* 2022, **50**(W1)**:** W216-221.

821

822 37. Komatsu M, Chiba T, Tatsumi K, Iemura S, Tanida I, Okazaki N*, et al.* A novel protein-
823 conjugating system for Ufm1, a ubiquitin-fold modifier. *Embo j* 2004, **23**(9)**:** 1977-1986.

824

825 38. Kang SH, Kim GR, Seong M, Baek SH, Seol JH, Bang OS*, et al.* Two novel ubiquitin-
826 fold modifier 1 (Ufm1)-specific proteases, UfSP1 and UfSP2. *J Biol Chem* 2007, **282**(8)**:**
827 5256-5262.

828

829 39. Tatsumi K, Sou YS, Tada N, Nakamura E, Iemura S, Natsume T*, et al.* A novel type of
830 E3 ligase for the Ufm1 conjugation system. *J Biol Chem* 2010, **285**(8)**:** 5417-5427.

831

832 40. Lemaire K, Moura RF, Granvik M, Igoillo-Esteve M, Hohmeier HE, Hendrickx N*, et al.*
833 Ubiquitin fold modifier 1 (UFM1) and its target UFBP1 protect pancreatic beta cells from
834 ER stress-induced apoptosis. *PLoS One* 2011, **6**(4)**:** e18517.

835

836 41. Chen C, Itakura E, Weber KP, Hegde RS, de Bono M. An ER complex of ODR-4 and
837 ODR-8/Ufm1 specific protease 2 promotes GPCR maturation by a Ufm1-independent
838 mechanism. *PLoS Genet* 2014, **10**(3)**:** e1004082.

839

840 42. Cai Y, Pi W, Sivaprakasam S, Zhu X, Zhang M, Chen J*, et al.* UFBP1, a Key Component
841 of the Ufm1 Conjugation System, Is Essential for Ufmylation-Mediated Regulation of
842 Erythroid Development. *PLoS Genet* 2015, **11**(11)**:** e1005643.

843

844 43. Wu J, Lei G, Mei M, Tang Y, Li H. A novel C53/LZAP-interacting protein regulates
845 stability of C53/LZAP and DDRGK domain-containing Protein 1 (DDRGK1) and
846 modulates NF-kappaB signaling. *J Biol Chem* 2010, **285**(20)**:** 15126-15136.

847

848 44. Jiang Y, Cheng Z, Mandon EC, Gilmore R. An interaction between the SRP receptor and
849 the translocon is critical during cotranslational protein translocation. *J Cell Biol* 2008,
850 **180**(6)**:** 1149-1161.

851

852 45. Song W, Raden D, Mandon EC, Gilmore R. Role of Sec61alpha in the regulated transfer
853 of the ribosome-nascent chain complex from the signal recognition particle to the
854 translocation channel. *Cell* 2000, **100**(3)**:** 333-343.

855

856 46. Mason N, Ciufo LF, Brown JD. Elongation arrest is a physiologically important function of
857 signal recognition particle. *Embo j* 2000, **19**(15)**:** 4164-4174.

858

859 47. Walter P, Blobel G. Translocation of proteins across the endoplasmic reticulum III.
860 Signal recognition protein (SRP) causes signal sequence-dependent and site-specific
861 arrest of chain elongation that is released by microsomal membranes. *J Cell Biol* 1981,
862 **91**(2 Pt 1)**:** 557-561.

863

864 48. Walczak CP, Leto DE, Zhang L, Riepe C, Muller RY, DaRosa PA*, et al.* Ribosomal
865 protein RPL26 is the principal target of UFMylation. *Proc Natl Acad Sci U S A* 2019,
866 **116**(4)**:** 1299-1308.

867

868 49. Wang L, Xu Y, Rogers H, Saidi L, Noguchi CT, Li H*, et al.* UFMylation of RPL26 links
869 translocation-associated quality control to endoplasmic reticulum protein homeostasis.
870 *Cell Res* 2020, **30**(1)**:** 5-20.

871

872 50. García-Suárez O, García B, Fernández-Vega I, Astudillo A, Quirós LM. Neuroendocrine
873 tumors show altered expression of chondroitin sulfate, glypican 1, glypican 5, and
874 syndecan 2 depending on their differentiation grade. *Front Oncol* 2014, **4:** 15.

875

876 51. Boztug K, Järvinen PM, Salzer E, Racek T, Mönch S, Garncarz W*, et al.* JAGN1
877 deficiency causes aberrant myeloid cell homeostasis and congenital neutropenia. *Nat*
878 *Genet* 2014, **46**(9)**:** 1021-1027.

879

880 52. Hwang S, Kim S, Kim K, Yeom J, Park S, Kim I. Euchromatin histone methyltransferase
881 II (EHMT2) regulates the expression of ras-related GTP binding C (RRAGC) protein.
882 *BMB Rep* 2020, **53**(11)**:** 576-581.

883

884 53. Xu L, Gao X, Yang P, Sang W, Jiao J, Niu M*, et al.* EHMT2 inhibitor BIX-01294 induces
885 endoplasmic reticulum stress mediated apoptosis and autophagy in diffuse large B-cell
886 lymphoma cells. *J Cancer* 2021, **12**(4)**:** 1011-1022.

887

888 54. Sheard MA, Asgharzadeh S, Liu Y, Lin TY, Wu HW, Ji L*, et al.* Membrane-bound TRAIL
889 supplements natural killer cell cytotoxicity against neuroblastoma cells. *J Immunother*
890 2013, **36**(5)**:** 319-329.

891

892 55. Mirandola P, Ponti C, Gobbi G, Sponzilli I, Vaccarezza M, Cocco L*, et al.* Activated
893 human NK and CD8+ T cells express both TNF-related apoptosis-inducing ligand
894 (TRAIL) and TRAIL receptors but are resistant to TRAIL-mediated cytotoxicity. *Blood*
895 2004, **104**(8)**:** 2418-2424.

896

897 56. Chen JJ, Knudsen S, Mazin W, Dahlgaard J, Zhang B. A 71-gene signature of TRAIL
898 sensitivity in cancer cells. *Mol Cancer Ther* 2012, **11**(1)**:** 34-44.

899

900 57. Sullivan GP, O'Connor H, Henry CM, Davidovich P, Clancy DM, Albert ML*, et al.* TRAIL
901 Receptors Serve as Stress-Associated Molecular Patterns to Promote ER-Stress-
902 Induced Inflammation. *Developmental Cell* 2020, **52**(6)**:** 714-730.e715.

903

904 58. Dufour F, Rattier T, Constantinescu AA, Zischler L, Morle A, Ben Mabrouk H*, et al.*
905 TRAIL receptor gene editing unveils TRAIL-R1 as a master player of apoptosis induced
906 by TRAIL and ER stress. *Oncotarget* 2017, **8**(6)**:** 9974-9985.

907

908 59. Lu M, Lawrence DA, Marsters S, Acosta-Alvear D, Kimmig P, Mendez AS*, et al.*
909 Opposing unfolded-protein-response signals converge on death receptor 5 to control
910 apoptosis. *Science* 2014, **345**(6192)**:** 98-101.

911

912 60. Iurlaro R, Puschel F, Leon-Annicchiarico CL, O'Connor H, Martin SJ, Palou-Gramon D*,*
913 *et al.* Glucose Deprivation Induces ATF4-Mediated Apoptosis through TRAIL Death
914 Receptors. *Mol Cell Biol* 2017, **37**(10).

915

916 61. van Raam BJ, Lacina T, Lindemann RK, Reiling JH. Secretory stressors induce
917 intracellular death receptor accumulation to control apoptosis. *Cell Death Dis* 2017,
918 **8**(10)**:** e3069.

919

920 62. Lam M, Marsters SA, Ashkenazi A, Walter P. Misfolded proteins bind and activate death
921 receptor 5 to trigger apoptosis during unresolved endoplasmic reticulum stress. *Elife*
922 2020, **9**.

923

924 63. Ramkumar P, Abarientos AB, Tian R, Seyler M, Leong JT, Chen M*, et al.* CRISPR-
925 based screens uncover determinants of immunotherapy response in multiple myeloma.
926 *Blood Adv* 2020, **4**(13)**:** 2899-2911.

927

928 64. Manzano M, Gunther T, Ju H, Nicholas J, Bartom ET, Grundhoff A*, et al.* Kaposi's
929 Sarcoma-Associated Herpesvirus Drives a Super-Enhancer-Mediated Survival Gene
930 Expression Program in Primary Effusion Lymphoma. *mBio* 2020, **11**(4).

931

932 65. De Leo A, Chen HS, Hu CC, Lieberman PM. Deregulation of KSHV latency conformation
933 by ER-stress and caspase-dependent RAD21-cleavage. *PLoS Pathog* 2017, **13**(8)**:**
934 e1006596.

935

936 66. Johnston BP, Pringle ES, McCormick C. KSHV activates unfolded protein response
937 sensors but suppresses downstream transcriptional responses to support lytic
938 replication. *PLoS Pathog* 2019, **15**(12)**:** e1008185.

939

940 67. Azfer A, Niu J, Rogers LM, Adamski FM, Kolattukudy PE. Activation of endoplasmic
941 reticulum stress response during the development of ischemic heart disease. *Am J*
942 *Physiol Heart Circ Physiol* 2006, **291**(3)**:** H1411-1420.

943

944 68. Zhang Y, Zhang M, Wu J, Lei G, Li H. Transcriptional regulation of the Ufm1 conjugation
945 system in response to disturbance of the endoplasmic reticulum homeostasis and
946 inhibition of vesicle trafficking. *PLoS One* 2012, **7**(11)**:** e48587.

947

948 69. Liu J, Wang Y, Song L, Zeng L, Yi W, Liu T*, et al.* A critical role of DDRGK1 in
949 endoplasmic reticulum homoeostasis via regulation of IRE1α stability. *Nature*
950 *Communications* 2017, **8**(1)**:** 14186.

951

952 70. Hu X, Pang Q, Shen Q, Liu H, He J, Wang J*, et al.* Ubiquitin-fold modifier 1 inhibits
953 apoptosis by suppressing the endoplasmic reticulum stress response in Raw264.7 cells.
954 *Int J Mol Med* 2014, **33**(6)**:** 1539-1546.

955

956 71. Tsherniak A, Vazquez F, Montgomery PG, Weir BA, Kryukov G, Cowley GS*, et al.*
957 Defining a Cancer Dependency Map. *Cell* 2017, **170**(3)**:** 564-576.e516.

958

959 72. Zhu H, Bhatt B, Sivaprakasam S, Cai Y, Liu S, Kodeboyina SK*, et al.* Ufbp1 promotes
960 plasma cell development and ER expansion by modulating distinct branches of UPR.
961 *Nature Communications* 2019, **10**(1)**:** 1084.

962

963 73. Hagelkruys A, Wirnsberger G, Stadlmann J, Wohner M, Horrer M, Vilagos B*, et al.* A
964 crucial role for Jagunal homolog 1 in humoral immunity and antibody glycosylation in
965 mice and humans. *J Exp Med* 2021, **218**(1).

966

967 74. Nosak C, Silva PN, Sollazzo P, Moon KM, Odisho T, Foster LJ*, et al.* Jagn1 Is Induced
968 in Response to ER Stress and Regulates Proinsulin Biosynthesis. *PLoS One* 2016,
969 **11**(2)**:** e0149177.

970

971 75. Charnaux N, Brule S, Hamon M, Chaigneau T, Saffar L, Prost C*, et al.* Syndecan-4 is a
972 signaling molecule for stromal cell-derived factor-1 (SDF-1)/ CXCL12. *Febs j* 2005,
973 **272**(8)**:** 1937-1951.

974

975 76. Farzan M, Babcock GJ, Vasilieva N, Wright PL, Kiprilov E, Mirzabekov T*, et al.* The Role
976 of Post-translational Modifications of the CXCR4 Amino Terminus in Stromal-derived
977 Factor 1α Association and HIV-1 Entry*. *Journal of Biological Chemistry* 2002, **277**(33)**:**
978 29484-29489.

979

980 77. Kremer KN, Peterson KL, Schneider PA, Meng XW, Dai H, Hess AD*, et al.* CXCR4
981 chemokine receptor signaling induces apoptosis in acute myeloid leukemia cells via
982 regulation of the Bcl-2 family members Bcl-XL, Noxa, and Bak. *J Biol Chem* 2013,
983 **288**(32)**:** 22899-22914.

984

985 78. Pham H, Kearns NA, Maehr R. Transcriptional Regulation with CRISPR/Cas9 Effectors
986 in Mammalian Cells. *Methods Mol Biol* 2016, **1358:** 43-57.

987

988 79. Pelossof R, Fairchild L, Huang CH, Widmer C, Sreedharan VT, Sinha N*, et al.* Prediction
989 of potent shRNAs with a sequential classification algorithm. *Nat Biotechnol* 2017, **35**(4)**:**
990 350-353.

991

992 80. Patil A, Manzano M, Gottwein E. CK1alpha and IRF4 are essential and independent
993 effectors of immunomodulatory drugs in primary effusion lymphoma. *Blood* 2018, **132**(6)**:**
994 577-586.

995

996 81. Bogerd HP, Whisnant AW, Kennedy EM, Flores O, Cullen BR. Derivation and
997 characterization of Dicer- and microRNA-deficient human cells. *Rna* 2014, **20**(6)**:** 923-
998 937.

999

1000 82. Martin M. CUTADAPT removes adapter sequences from high-throughput sequencing
1001 reads. *EMBnetjournal* 2011, **17**.

1002

1003 83. Langmead B, Trapnell C, Pop M, Salzberg SL. Ultrafast and memory-efficient alignment
1004 of short DNA sequences to the human genome. *Genome Biology* 2009, **10**(3)**:** R25.

1005

1006 84. Li W, Xu H, Xiao T, Cong L, Love MI, Zhang F*, et al.* MAGeCK enables robust
1007 identification of essential genes from genome-scale CRISPR/Cas9 knockout screens.
1008 *Genome Biol* 2014, **15**(12)**:** 554.

1009

1010 85. Cock PJA, Antao T, Chang JT, Chapman BA, Cox CJ, Dalke A*, et al.* Biopython: freely
1011 available Python tools for computational molecular biology and bioinformatics.
1012 *Bioinformatics* 2009, **25**(11)**:** 1422-1423.

1013

1014 86. Clement K, Rees H, Canver MC, Gehrke JM, Farouni R, Hsu JY*, et al.* CRISPResso2
1015 provides accurate and rapid genome editing sequence analysis. *Nature Biotechnology*
1016 2019, **37**(3)**:** 224-226.

1017

1018 87. Livak KJ, Schmittgen TD. Analysis of relative gene expression data using real-time
1019 quantitative PCR and the 2(-Delta Delta C(T)) Method. *Methods* 2001, **25**(4)**:** 402-408.

1020

1021 88. Virtanen P, Gommers R, Oliphant TE, Haberland M, Reddy T, Cournapeau D*, et al.*
1022 Author Correction: SciPy 1.0: fundamental algorithms for scientific computing in Python.
1023 *Nature Methods* 2020, **17**(3)**:** 352-352.

1024

1025 89. Waskom M. seaborn: statistical data visualization. *JOSS* 2021, **6**(60)**:** 3021.

1026

1027 90. Zhou F, Shimoda M, Olney L, Lyu Y, Tran K, Jiang G*, et al.* Oncolytic Reactivation of
1028 KSHV as a Therapeutic Approach for Primary Effusion Lymphoma. *Mol Cancer Ther*
1029 2017, **16**(11)**:** 2627-2638.

1030

1031 **Figures**

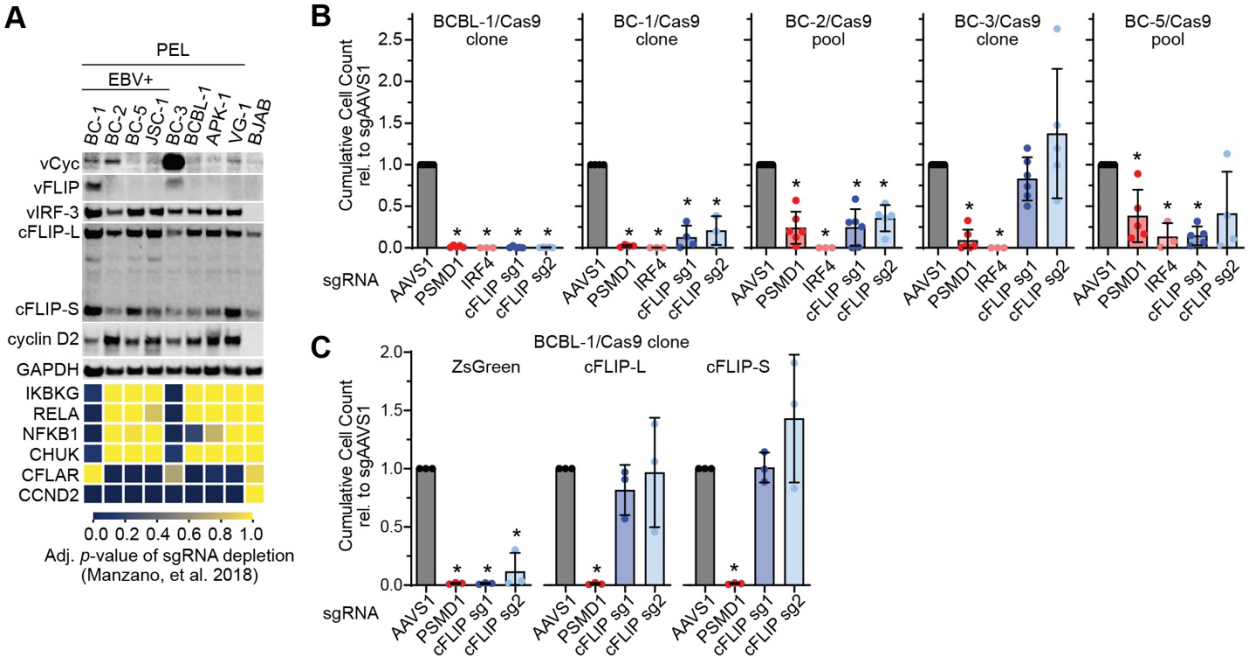

1032

1033 **Fig. 1** cFLIP is broadly essential in PEL cell lines. **A.** Top: Cell lysates from the indicated PEL
1034 cell lines or KSHV-negative BJAB cells were analyzed by Western blotting for the indicated
1035 proteins. The cFLIP splice variants cFLIP-L and cFLIP-S are marked. Bottom: Heatmap of
1036 depletion for sgRNAs targeting the indicated genes, using data from Manzano, et al. 2018.
1037 Lower FDR-adjusted *p*-values of depletion indicate significant sgRNA depletion in the screens,
1038 suggesting essential or fitness roles. **B.** Cas9-expressing PEL cell lines were transduced with
1039 the indicated sgRNAs at MOI 3 and selected with puromycin. Graphs show the endpoints (day
1040 8-10) of cumulative cell growth curves relative to an sgRNA targeting the safe harbor locus
1041 AAVS1 (see Material and Methods). sgRNAs targeting PSMD1 and IRF4 are controls for other
1042 essential genes. Error bars represent SD (n = 4-6 independent repeats). For Western Blot
1043 control, see Fig. S1C. **C.** BCBL-1/Cas9 expressing ZsGreen, sgRNA-resistant cFLIP-L, or
1044 sgRNA-resistant cFLIP-S were challenged with the indicated sgRNAs. Error bars represent SD
1045 (n = 3 independent repeats). For Western Blot control, see Fig. S1E. In panels B and C,
1046 statistical significance for loss of cell viability compared to sgAAVS1 was analyzed using one-
1047 sided, one-sample t-testing (* denotes FDR-adjusted p <= 0.05), FDR-adjusted p-values are
1048 listed in Table 6. Rescue in panel C was significant as determined using a one-sided,
1049 independent two-sample t-test, with FDR-adjusted p-values listed in Table S6.

1050

1051

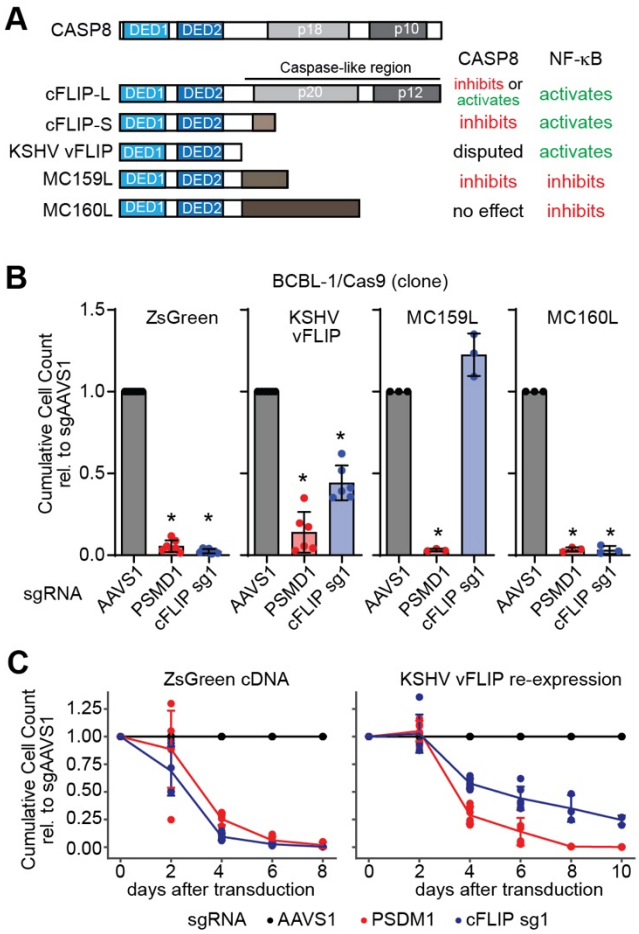

Fig. 2 cFLIP and KSHV vFLIP are functionally distinct in PEL cell lines. **A.** Schematic representation of human CASP8, the cFLIP-L/S splice variants, KSHV vFLIP, and the MCV FLIP proteins MC159L and MC160L. Also shown are the characterized activities of each protein towards CASP8/the extrinsic apoptosis pathway and the NF-κB pathway. **B.** BCBL-1/Cas9 expressing ZsGreen, KSHV vFLIP, MCV MC159L, or MCV MC160L were challenged with the indicated sgRNAs. Analyses of cumulative growth curve experiments on day 6 after sgRNA transduction are shown. Error bars represent SD (n = 3 independent repeats). For Western Blot controls, see Fig. S2. Statistical significance for loss of cell viability compared to sgAAVS1 was analyzed using one-sided, one-sample t-testing (* denotes FDR-adjusted p <= 0.05). Rescue by expression of KSHV vFLIP and MCL159L was significant as determined using a one-sided, independent two-sample t-test. FDR-adjusted p-values are listed in Table S6. **C.** Extended growth curves for the ZsGreen and KSHV vFLIP data in panel B show that vFLIP rescue is significant, but not efficient. For details on statistical analysis see Table S6 and Material and Methods section.

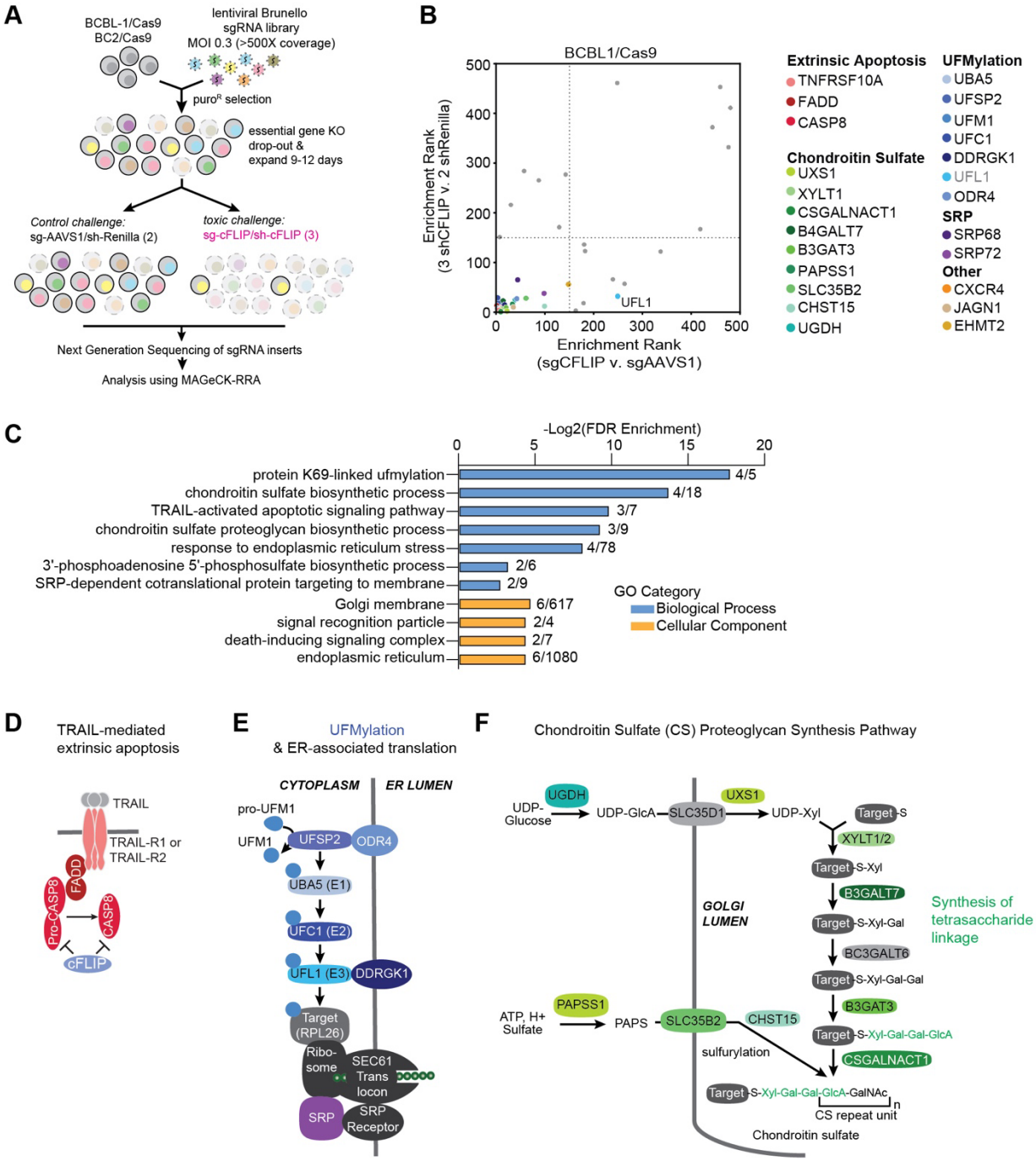

Fig. 3. Genome-wide synthetic rescue screens uncover components of the death program repressed by cFLIP in PEL cells. **A.** Experimental design for CRISPR-based synthetic rescue screening. **B.** Results of the BCBL-1 resistance screens. Shown are the gene-level ranks output by MAGeCK-RRA based on library sgRNA enrichment after the toxic cFLIP shRNA challenge (y-axis) or the toxic cFLIP sgRNA-challenge (x-axis) relative to matched negative control perturbations. For clarity, only the top 500 hits in each screen are displayed. UFL1 was highlighted as a UFMylation pathway gene but does not pass our analysis cutoff. **C.** DAVID pathway analysis of the 23 high confidence hits obtained by intersecting the top 150 hits each from the BCBL-1 sgRNA and shRNA screens. Numbers at right show number of hits from each

1076 pathway. For complete DAVID output, see Table S3. **D.** Diagram of canonical death signaling
1077 via TRAIL through TRAIL receptors. Hits are colored as in panel B. **E.** Diagram of the
1078 UFMylation and ER-associated translation pathways, screening hits are colored as in panel B.
1079 UFM1 is cytoplasmic, but the UFM1 conjugation machinery is anchored on the cytoplasmic face
1080 of the ER membrane by adaptors ODR4 and DDRGK1 (UFBP1). RPL26 is the main
1081 characterized substrate for UFMylation and impacts translational pausing during ER-associated
1082 degradation. The SRP complex is involved in protein translocation and initiates translational
1083 pausing. **F.** Diagram of the Chondroitin sulfate (CS) proteoglycan synthesis pathway, screen
1084 hits are colored as in panel B.

1085

1086

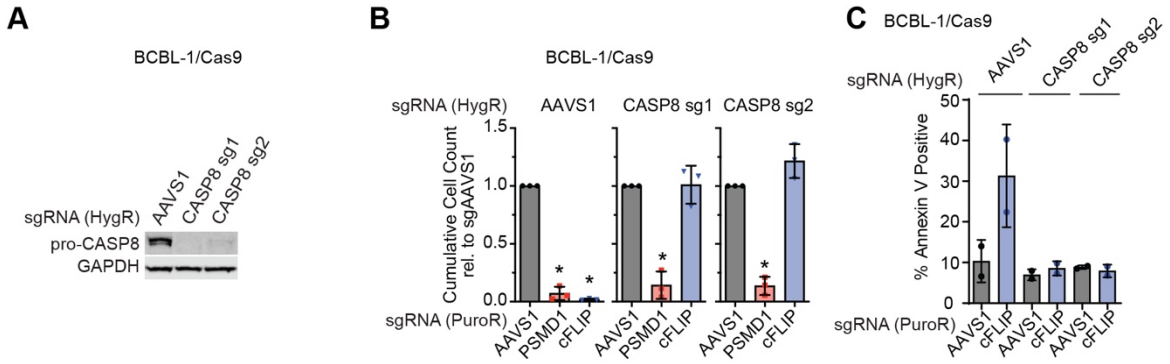

1087

1088 **Fig. 4** Cellular FLIP protects PEL cells from CASP8-induced cell death. **A.** BCBL-1/Cas9 cells
1089 were transduced with the indicated sgRNAs, selected with hygromycin, and knockout of CASP8
1090 was confirmed by Western blot. **B.** The cell lines from panel A were challenged with puromycin
1091 resistant lentiviral sgRNA vectors at equal MOI and cumulative growth curve analyses were
1092 performed as previously. Error bars represent SD from 3 independent repeats. For Western Blot
1093 controls, see Fig. S4D. Statistical significance for loss of cell viability compared to sgAAVS1
1094 was analyzed using one-sided, one-sample t-testing (* denotes FDR-adjusted p <= 0.05).
1095 Rescue by CASP8 KO was significant as determined using a one-sided, independent two-
1096 sample t-test. FDR-adjusted p-values are listed in Table S6. **C.** Cells were challenged with
1097 control or cFLIP sgRNAs as in panel B, but not selected with puromycin, and stained with
1098 Annexin V 48 hours after transduction (n=2 independent repeats, error bars indicate range).

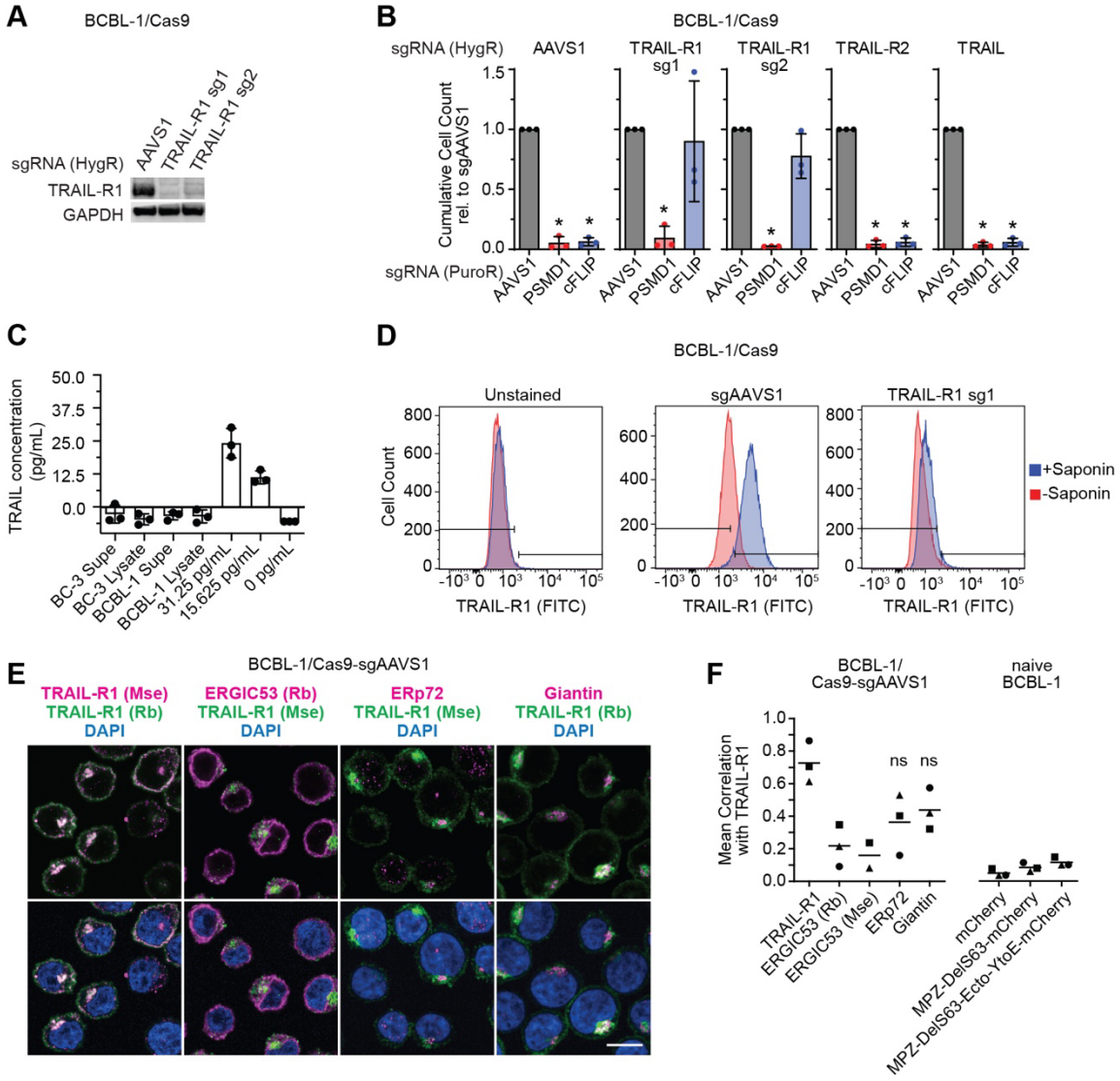

Fig. 5. Cellular FLIP protects PEL cells from a ligand-independent, intracellular TRAIL-R1-mediated cell death program. **A.** BCBL-1/Cas9 cells were transduced with the indicated sgRNAs, selected with hygromycin, and knockout of TRAIL-R1 was confirmed by Western blot. **B.** Cell lines depicted in panel A were challenged with puromycin resistant lentiviral sgRNA vectors at equal MOI and cumulative growth curve analyses were performed as previously. Error bars represent SD from 3 independent repeats. For Western Blot control, see Fig. S5A. Statistical significance for loss of cell viability compared to sgAAVS1 was analyzed using one-sided, one-sample t-testing (* denotes p<= 0.05). Rescue by TRAIL-R1 KO, but not TRAIL-R2 or TRAIL KO, was significant as determined using one-sided, independent two-sample t-tests. FDR-adjusted p-values are listed in Table S6. **C.** BC-3 or BCBL-1 cells were plated at $2x10^5$ cells/mL, and supernatants or lysates were harvested 3 days later and used for anti-TRAIL ELISA assay. Known concentrations of recombinant human TRAIL confirm sensitivity down to the ~10 pg/mL range. **D.** Knockout cell lines were fixed in 4% FA and stained for TRAIL-R1 with or without permeabilization by saponin. Shown at left are unstained control cells. Quantification over 3 independent repeats can be found in Fig. S6C. **E.** Representative images to establish colocalization of TRAIL-R1 with itself, using a positive control antibody directed against a

1116 different epitope, the ERGIC marker ERGIC53, the ER marker ERp72, and the Golgi marker
1117 Giantin. TRAIL-R1 is shown in green with other markers in magenta to depict overlapping signal
1118 as white. See Fig. S5E for results from a second ERGIC53 antibody and TRAIL-R1 KO cells.
1119 Scale bar = 10μm. Mse and Rb indicate antibodies raised in mice or rabbits, respectively. **F.** 3D
1120 colocalization of TRAIL-R1 with the indicated proteins was quantified using Pearson's
1121 correlation coefficients (PCCs, n=3 independent repeats, except n=2 for mouse anti-ERGIC53).
1122 Representative images are shown in Figs. 5E, S5D-E. We quantified an average of ~1800 cells
1123 per replicate. Statistical significance of the difference from TRAIL-R1 self-colocalization
1124 detected with two different TRAIL-R1-specific antibodies was determined by two-sided,
1125 independent two-sample t-test (* <=0.05). All markers other than ERp72 and Giantin (indicated
1126 by ns) were significantly less colocalized with TRAIL-R1 than TRAIL-R1 self-colocalization.

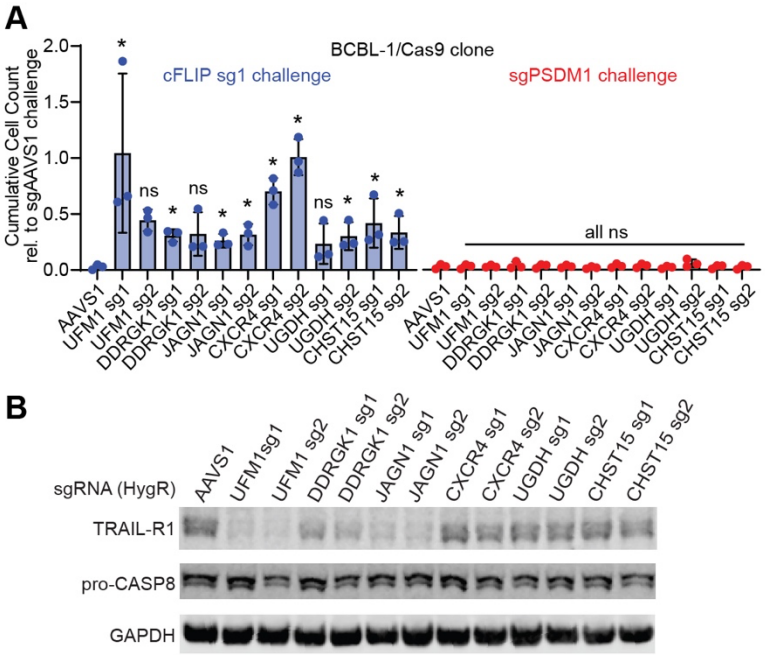

Figure 6. Knockdown of genes that participate in UFMylation, the chondroitin sulfate synthesis pathway, or of JAGN1 and CXCR4 overcome cFLIP dependency in PEL cells. **A.** Single-gene knockout pools were generated as previously for two genes each in the UFMylation and chondroitin sulfate biosynthesis pathway along with CXCR4 and JAGN1 and these cell lines were used to perform cumulative growth curves following transduction with a second sgRNA as previously. Statistical significance of rescue from cFLIP sg1 induced cell death was determined using one-sided, independent two-sample t-tests (* denotes FDR-adjusted p <= 0.05). FDR-adjusted p-values and statistical significance of loss of viability are listed in Table S6. Western controls are in Fig. S6B. **B.** Single-gene KO pools were analyzed for TRAIL-R1 and pro-caspase 8 expression by Western blotting.